Applicability of Existing Photovoltaic Module Temperature Model Parameters to Bifacial Solar Panels

Master of Science in Technology Thesis
University of Turku
Department of Mechanical and Materials Engineering
Materials Engineering
Materials of Energy Technology

Author:
Julianna Varjopuro

21.3.2025
Turku

Master of Science in Technology Thesis
University of Turku

Subject: Materials Engineering
Author: Julianna Varjopuro
Title: Applicability of Existing Photovoltaic Module Temperature Model Parameters to Bifacial Solar Panels
Supervisor(s): M.Sc. (Tech.) Aleksi Kamppinen, Dr. Aapo Poskela, and Prof. Kati Miettunen
Number of pages: 64 pages
Date: 21.3.2025

Abstract.

The bifacial solar cell technologies have been gaining interest in renewable energy sector due to their ability to absorb irradiance from both front and rear surfaces and, thus, increase the total energy production. In addition, the vertically installed bifacial panels can be used to balance the mismatch between energy consumption and production. Modeling the operation of commercial solar panels is important for predicting both instantaneous and long-term performance, but also for comparing the profitability of various technologies. Due to the temperature dependence of electrical efficiency, understanding the thermal behavior of solar panels is essential. In the performance models of bifacial solar panels, the impact of operating temperature on efficiency is often estimated using semi-empirical temperature models initially designed for monofacial panels. However, the applicability of these temperature model parameters to bifacial panels has not been extensively studied.

In this thesis, the thermal model, built using COMSOL Multiphysics, and the PVLib irradiance model are applied to simulate the operating temperatures of solar panels with different installation configurations in varying ambient conditions. The simulated temperature data is used to determine the parameters of common temperature models (Sandia, Faiman, Mattei, TRNSYS). The main objective of this thesis is to evaluate the suitability of common temperature model parameters, initially designed for monofacial solar panels, for estimating the operating temperature of bifacial panels. Moreover, the aim is to compare the accuracy of temperature model estimations with different inputs for irradiance.

The results confirm that the temperature of bifacial panels can be estimated with good accuracy using the model parameters of monofacial panels if the tilt angles of the panels are similar. However, the model parameters of vertical panels are about 10–30 % higher than those of tilted panels. Furthermore, the results present that the most accurate temperature estimations are obtained by applying either experimentally or computationally determined plane of array irradiance (POA) to the models. The use of global horizontal irradiance (GHI) as a model input for irradiance cannot be recommended.

Key words: thermal modeling, bifacial photovoltaics, temperature model parameters

Diplomityö
Turun yliopisto

Oppiaine: Materiaalitekniikka
Tekijä: Julianna Varjopuro
Otsikko: Yleisten aurinkosähkömoduulien lämpömalliparametrien soveltuvuus kaksipuoleisille aurinkopaneeleille
Ohjaaja(t): DI Aleksi Kamppinen, TkT Aapo Poskela ja Prof. Kati Miettunen
Sivumäärä: 64 sivua
Päivämäärä: 21.3.2025

Tiivistelmä

Kaksipuoleiset aurinkokennoteknologiat ovat kasvavan kiinnostuksen kohteena uusiutuvan energiantuotannon alalla, koska ne pystyvät absorboimaan säteilyä myös takapinnaltaan ja siten kasvattamaan energian kokonaistuotantoa. Lisäksi vertikaalisesti asennettuja kaksipuoleisia paneeleja voidaan hyödyntää energiankulutuksen ja -tuotannon tasapainottamiseen. Kaupallisten aurinkopaneelien toiminnan mallintaminen on tärkeää sekä reaaliaikaisen että pitkän aikavälin suorituskyvyn ennustamiseksi, mutta myös erilaisten teknologioiden kannattavuuden vertailemiseksi. Sähköisen hyötysuhteen lämpötilariippuvuuden vuoksi ymmärrys aurinkopaneelien lämpökäyttäytymisestä on olennaista. Useissa kaksipuoleisten aurinkopaneelien tehomalleissa toimintalämpötilan vaikutusta hyötysuhteeseen arvioidaan käyttäen alun perin yksipuoleisille paneeleille suunniteltuja puoliempiirisiä lämpömalleja. Näiden lämpömallien parametrien soveltuvuutta kaksipuoleisille paneeleille ei ole kuitenkaan laajasti tutkittu.

Tässä opinnäytetyössä sovelletaan COMSOL Multiphysics -ohjelmalla luotua lämpömallia sekä PVLib-säteilymallia eri kallistuskulmiin asennettujen aurinkopaneelien toimintalämpötilojen simuloimiseen vaihtelevissa ympäristön olosuhteissa. Simuloitua lämpötiladataa hyödynnetään yleisten lämpömallien (Sandia, Faiman, Mattei, TRNSYS) parametrien määrittämiseen. Opinnäytetyön keskeisenä tavoitteena on arvioida yksipuoleisille paneeleille suunniteltujen lämpömalliparametrien soveltuvuutta kaksipuoleisien aurinkopaneelien lämpötilan ennustamiseen. Lisäksi tavoitteena on vertailla lämpömalliennusteiden tarkkuutta erilaisilla säteilyn syötteillä.

Tulokset vahvistavat, että kaksipuoleisten paneelien lämpötila voidaan ennustaa hyvällä tarkkuudella käyttäen yksipuoleisten paneelien malliparametrejä, mikäli paneelien kallistuskulmat ovat samanlaiset. Toisaalta pystysuuntaisten paneelien malliparametrien arvot ovat noin 10–30 prosenttia suurempia kuin kallistettujen paneelien vastaavat. Lisäksi tulokset osoittavat, että tarkimmat lämpötilaennusteet saadaan, kun säteilyn syötteenä käytetään paneeliin saapuvaa kokonaissäteilyä (POA), joka on määritetty joko kokeellisesti tai laskennallisesti. Horisontaalista kokonaissäteilyä (GHI) taas ei voida suositella käytettäväksi säteilyn syötteenä.

Avainsanat: Lämpömallinnus, kaksipuoleiset aurinkopaneelit, lämpömalliparametrit

Acknowledgment

I thank my supervisors, M.Sc. (Tech) Aleksi Kamppinen, Dr. Aapo Poskela, and Prof. Kati Miettunen, for their patient guidance and feedback throughout this M.Sc. thesis project. I am grateful to Professor Miettunen for her insightful ideas and support, as well as the opportunity to work and write this thesis within Solar Energy Materials and Systems group. I thank the Research Council of Finland (RealSolar-project, 358542) for funding this work, and Finnish Meteorological Institute and New Energy Research Center (TUAS) for kindly providing measurement data. Finally, I want to express my gratitude to my family for their continuous encouragement throughout my studies. Special thanks to my husband for all the emotional support and for keeping me going by always making me coffee.

Contents

List of Figures

List of Tables

1 Introduction

Solar energy has been a rising trend for years [1], [2]. However, the focuses and challenges of solar energy technologies have changed over time. In the past the focus was on increasing the efficiency of the modules and the challenges were related to the reasonable cost of the produced energy. Nowadays energy storage solutions and balancing the consumption with production have increasingly become the focus of research along with improving the efficiency. In addition, new photovoltaic (PV) technologies have entered the market. One such technology is bifacial photovoltaics.

Bifacial cells were first introduced decades ago but their widespread commercial adoption did not start until the 2010s [3]. This cell technology can absorb irradiance from both front and rear surfaces [4]. Currently, the share of bifacial PV (BPV) panels with bifacial cells in the market is constantly increasing. In year 2017, less than 5 percent of the panels in the market were bifacial whereas in year 2032 the corresponding percent is expected to be around 60 percent [5], [6]. The share of bifacial cells is even higher since bifacial cells can be used also in traditional monofacial PV (MPV) panels [5]. Bifacial panels are interesting technology for many reasons, one of which is the possibility to generate more energy using the same area of land as the monofacial panels [7]. Another advantage of bifacial panels is the wider variety of installation configurations. For instance, the vertical mounting of BPV enable to shift the production peak from noon to morning and evening, when the energy demand of households is typically at the highest. This decreases the mismatch between electricity consumption and production [7].

Understanding the operation of commercial PV power system is essential for accurately estimating both instantaneous power production, and long-term performance. Power prediction models allow the assessment of system profitability in various PV applications and the comparison of different technologies [7], [8]. For instance, the benefits of bifacial systems with different installation configurations at certain geographical locations can be evaluated [7]. The knowledge about the thermal behavior of PV panels is relevant, among other things, for the performance modeling because the efficiency of solar cells is temperature-dependent [9].

One challenge with the PV thermal modeling is that the operating temperature depends on the irradiance received by the surface(s) of the panel which in turn depends on multiple factors, including the ambient conditions, geographical location, season and time of day as well as the

mounting of the panel [10]. Physical device thermal models in which the model includes information about the material properties and boundary conditions of the system are relatively heavy in terms of computational resources. Therefore, the common PV temperature models, that predict the operating temperatures using only easily accessible meteorological data, are interesting from the performance modeling point of view. These common PV temperature models are initially designed for the traditional monofacial panels, but they are also utilized for temperature predictions of bifacial PV panels [9], [11], [12]. However, the suitability of these models and their model parameters for predicting the temperature of bifacial panels has not been broadly studied [13], [14].

With that being said, this thesis aims to answer two questions related to the temperature estimations of bifacial solar panels. The first research question is: Are common PV temperature models and model parameters, that are initially determined for monofacial PV panels, suitable for estimating the operating temperatures of bifacial panels? To address this question, common PV temperature model parameters were first determined for monofacial panel and both tilted and vertical bifacial panels using the simulated temperature data, followed by a comparison of these parameters.

The second research question is: Can global horizontal irradiance (GHI) be effectively utilized in temperature estimation models instead of the commonly used plane of array (POA) irradiance? Furthermore, how accurate temperature estimation can be obtained using the POA irradiance calculated from GHI instead of the measured one? These are interesting questions because GHI data is more easily accessible than the measured POA irradiance data. Availability of measured POA irradiance data is more limited because the irradiance received by the tilted surface depends on the system specifications, such as the tilt angle of the panel, and thus, it must be measured separately for each case. GHI, on the other hand, is the total irradiance received by a horizontal surface and it is much more straightforward to measure. Further, the POA irradiance can be quite effectively calculated from GHI data, using common decomposition and transposition models that are discussed later in this thesis. It is assumed that when using GHI or the calculated POA as a model input for irradiance, the accuracy of model is somewhat lower than when using the measured POA irradiance. However, for the needs of some target groups, such as household level consumers, a reasonably accurate model would be sufficient. Furthermore, if GHI and the calculated POA could be effectively used in temperature estimations, the challenges associated with the availability of measured POA irradiance data will be eased.

To achieve the objectives of the thesis, a physical device thermal model, combined with an irradiance model, was build. The physics-based thermal model allows the comparison of the thermal behavior of mono- and bifacial silicon panels under different ambient conditions, mounting configurations and locations. The thermal models were validated with the experimental measurement data from mono- and bifacial panels. The data simulated with thermal models was used to assess the applicability of common PV temperature models to bifacial panels and the use of GHI and calculated POA irradiance as an input value for those temperature models.

The thesis is organized as follows: Section 2 briefly describes the characteristics and applications of bifacial panels. Section 3 discusses the existing literature regarding the performance, irradiance, and thermal modeling of bifacial PV on which this thesis relies. Section 4 introduces the chosen methods for building a physics based thermal model for mono- and bifacial photovoltaic panels. Additionally, the results of model validation are presented. Section 5 reveals the differences in the operation temperatures of mono- and bifacial panels with different installations in varying ambient conditions. Furthermore, the temperature model parameters of both panel types are determined, and the accuracy of temperature predictions using GHI and the calculated POA irradiance are investigated. Section 6 discusses the limitations of the study. Finally, Section 7 concludes the main results.

2 Overview of bifacial photovoltaic technology

2.1 Bifacial cells and modules

Similar to traditional monofacial PV panels, bifacial PV panels operate by converting solar radiation into voltage and current via phenomenon known as the photovoltaic effect [3]. The photovoltaic effect occurs under illumination. It relies on the photons of light to excite electrons of the semiconductor material from valence band to conduction band, creating electron-hole pairs [3], [15]. The internal electric field separates the electrons and holes. The electrons flow to n-type semiconductor and holes to p-type semiconductor which creates a voltage difference across the cell. When front and rear contacts of the cell are connected, electrons flow through the external circuit and generate a current [3], [15].

The differences in operation of mono- and bifacial PV modules are mainly due to the fact that the bifacial cells can absorb irradiance from both sides [3], [16], [17]. To enable bifacial absorption, the back contacts in bifacial cells are transparent or localized unlike the back contacts in monofacial cells which are non-transparent and completely cover the rear surface. Moreover, the back cover of the BPV module needs to be either glass or transparent organic material [3].

Aluminium back surface field (Al-BSF) cells (Figure 1d) used to be the dominant cell type on the MPV market, but nowadays they are often replaced with the monofacial passivated emitter rear contact (PERC) cells (Figure 1b). As the market share of bifacial PV modules increases, the BPV cell technologies, such as bifacial PERC (Figure 1a) and heterojunction with intrinsic thin-layer (HIT) solar cells (Figure 1c), become increasingly relevant [16]. The structure of mono- and bifacial PERC cells is similar, but bifacial PERC cells differ from the monofacial ones in their rear contact design [16]. Both mono- and bifacial PERC cells consist of the front silver (Ag) contacts, front and rear passivating coatings that also act as an anti-reflection (AR) coating, n+ emitter, p-type silicon, local Al-BSF and rear Al contacts [16], [17]. The structure of HIT cells is somewhat different from the other cell types presented. HIT cells use carrier-selective passivating contact structures with advantages such as lower recombination losses. n- and p-type doped silicon layers are responsible for the surface selectivity whereas the intrinsic amorphous silicon provides the surface passivation. The other components of HIT cells are front and rear Ag-contacts, front and rear transparent conductive oxide (TCO) layer and n-type silicon [16]. In addition, there are also other promising cell technologies for BPV modules,

including passivated emitter rear locally-diffused (PERL), passivated emitter rear totally diffused (PERT) [3], [16], [17], and tunnel oxide passivated contacts (TOPCon) cells [16], [18]. PERT cells, that utilize n-type silicon, have drawn attention because of their high efficiency [16]. Moreover, TOPCon cells are expected to become the most popular cell technology in the PV market [19]. TOPCon cells utilize n-type silicon with a tunnel oxide layer which act as a passivating layer, and they have both high bifaciality and efficiency [19].

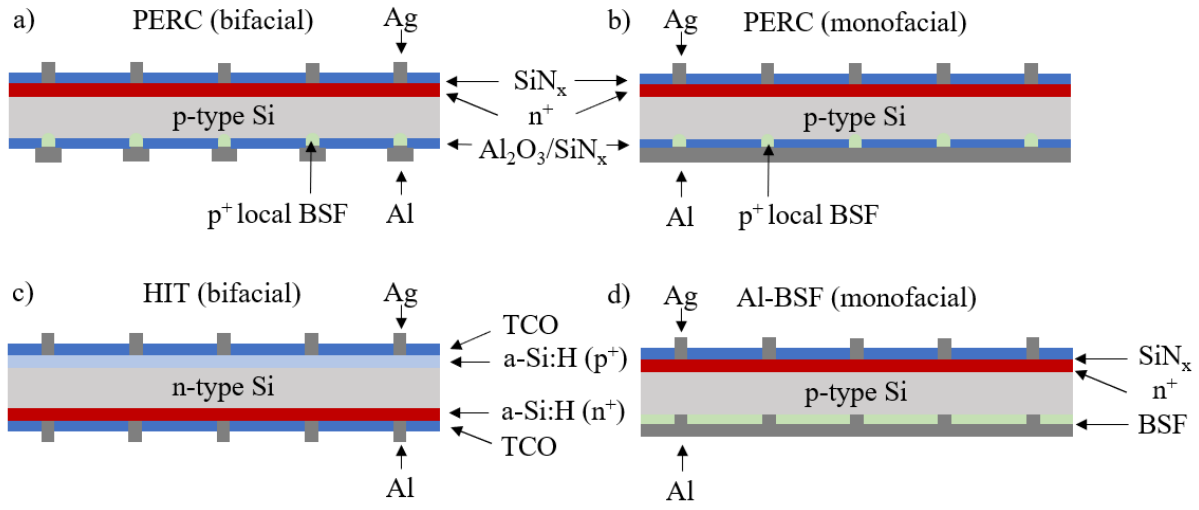

Figure 1: Structures of common PV cell types including (a, b) mono- and bifacial PERC, (c) bifacial HIT and (d) monofacial Al-BSF cells [16], [17].[16], [17]

Aforementioned cell types have different physical properties due to different materials and structures. These physical properties, including the temperature coefficient, bifaciality, and sub-bandgap absorption, affect the perfomance of PV module [9]. The temperature coefficient determines how much the efficiency of cell decreases when the temperature increases by one degree. It is stated that the temperature coefficient varies for different the cell technologies and, for example, the HIT cells have significantly lower temperature coefficient than Al-BSF cells [9]. Furthermore, the bifaciality determines the ratio of the rear side performance to the front side performance and the higher bifaciality thus leads to the higher efficiency of the cell [16]. The bifaciality of PERC cells is reported to range between 70 and 80 % whereas the bifaciality of HIT is typically over 95 % [16], [17]. Sub-bandgap absorption in turn affects the rate at which of temperature changes [9]. It refers to the fraction of irradiance with the photon energy lower than the band gap energy that is absorbed, for instance, by the metal contact of the cell [9]. The bifacial cells have lower sub-bandgap absorption than monofacial cells, due to the smaller area of rear metal contact [20]. Reduced sub-bandgap absorption means that the heating is lower in comparison with the monofacial cells [9]. The temperature coefficient, bifaciality,

and front and rear efficiency of common PV cell types are shown in Table 1. These properties vary considerably between cell types (Table 1). For this reason, the type of cell used in PV module is a noteworthy factor for both temperature and performance predictions.

Table 1: Temperature coefficient, bifaciality and efficiency of common cell types used in PV modules

	TC [% / °C]	BF [%] ^	η_{front} | η_{rear} [%] *
Al-BSF	-0.41–0.43 [9], [21], [22]	-	16.8 [9]
mono-PERC	-0.39 [21]	-	18.6–22.5 [16], [23]
bi-PERC	-0.34–0.35 [18], [22]	70–80 [3], [17]	19.4–21.2 [17]| 16.7–18.1 [17]
HIT	-0.26–0.27 [9], [18]	83–100 [3], [16], [17], [18]	24.7 [17] | -
PERT	-0.33 [24], [25]	80–95 [3], [16], [17]	19.5–22 [17]| 17–19 [17]
PERL	-	80–89 [3], [17]	19.8 [17] | -
TOPCon	−0.32 [18]	76 [18]	22-25 [19] | -

^ The bifaciality is not reported for Al-BSF and mono-PERC because they are monofacial.
* The vertical bar separates the efficiencies of front and rear surface of the cell. If literature value was not found, the number is replaced by -.

2.2 Applications of bifacial photovoltaics

Bifacial solar panels have a wide variety of possible installation configurations, such as tilted and vertical mounting, which each offer different benefits. For instance, the vertically mounted bifacial panels (VBPV) transfer the energy production peak from solar noon to morning and evening, which improves the balance between the electricity production and demand [7]. At the Nordic latitudes, where the sun elevation angle is often low, the vertical mounting is an effective option [26]. Of different azimuth angles of VBPV panels, the east and west oriented panels show best performance [7]. The VBPV panels are advantageous from the land use point of view, as they can be applied, for instance, to noise barriers, balconies, and other urban infrastructure (Figure 2) [3]. The challenge with the east-west mounted vertical panels is the shading from the surrounding due to low sun elevation angles. While the VBPVs are functional in Nordic conditions, the conventionally mounted bifacial panels (CBPV) outperform those in most geographical locations [7], [26]. CBPV panels are recommended to be installed the front side towards the south. The optimal tilt and azimuth angle of the panel depends, among other things, on the latitude of installation site [26]. The bifacial tilted panels benefit from high reflectivity i.e., albedo, of an environment if they are installed at a sufficient distance from the background [12]. For example, bus stations and other things with open shelters are suitable for CBPV [3], [7]. In addition, bifacial panels can be installed on the roof tops like traditional monofacial ones.

Overall, bifacial solar panels provide a practical solution for energy production, especially in northern latitudes [7]. On a global scale, studies show that the levelized cost of energy for the CBPV panels is lower than that of the monofacial panels above latitude of 40°. In contrast, the VBPV panels become more economically profitable above latitude of 65° [7].

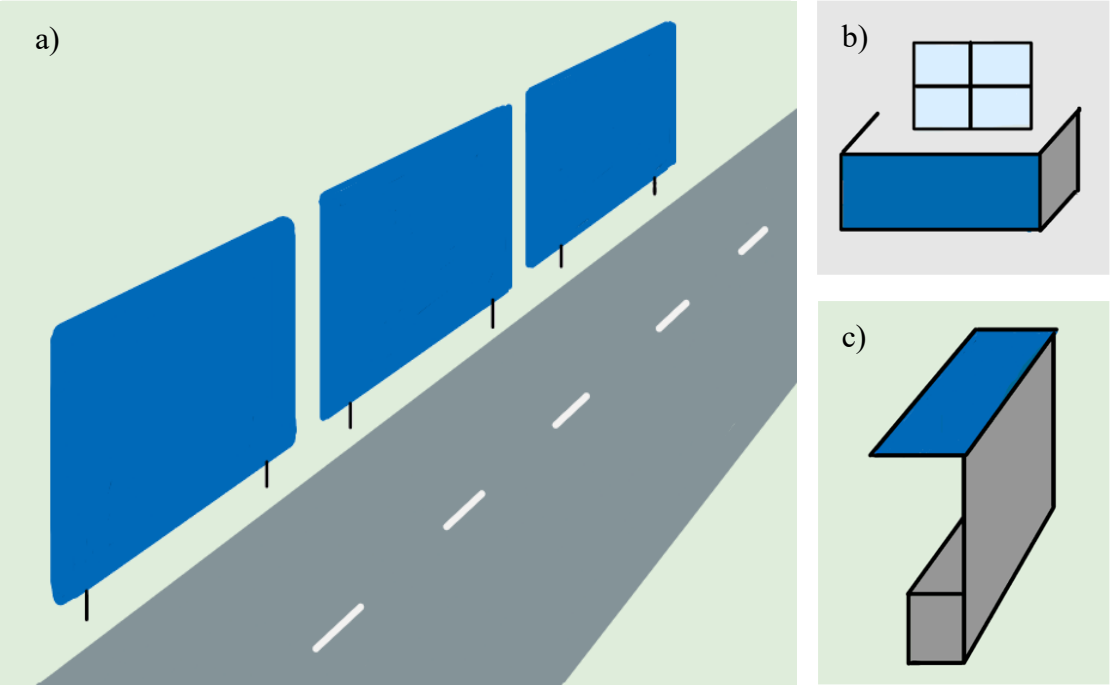

Figure 2: Potential applications of bifacial PV panels with different installation configurations, including a) noise barriers, b) balconies, and c) bus stops.

3 Existing work on modeling photovoltaic modules

3.1 Photovoltaic module performance models

Some studies that solely focus on the thermal modeling of bifacial PV panels are found in literature [27], [28], [29], [30], [31]. Thermal behavior of PV panels is also discussed in the majority of performance models because the operating temperature, together with the irradiance, is so relevant for the operation of PV panels. Thus, to get a broader understanding of both temperature and irradiance modeling as well as the relationship between temperature and efficiency, looking into the research regarding performance modeling is useful.

Several performance models of bifacial PV modules have been described in literature [9], [10], [11], [12], [13], [32], [33], [34], [35]. These models allow to simulate the impact of different environmental conditions, geographical locations, and module configuration on the performance of the PV panel to varying degrees. For example, the models by Yusufoglu et al. [32] and Janssen et al. [33] simulate the performance of BPV on specific locations whereas the models by Patel et al. [9] and Sun et al. [12] allow to account the different locations all around the world.

Furthermore, the aforementioned performance models consider the irradiance received by the panel using various methods with different accuracies. The availability of solar irradiance data for specific panel orientations and tilt angles is often limited and, therefore, the global horizontal irradiance (GHI) is commonly used to estimate other components of solar irradiance [36]. There are several decomposition models for splitting the GHI to direct normal irradiance (DNI) and diffuse horizontal irradiance (DHI) components, including Orgill Hollands [37] and Erbs [38] models as well as Perez [39] and Reindl [40] family models. Perez1 decomposition model [39] is also referred to as DIRINT model. The DIRINT model is estimated to be among the ten best performing models in the Nordic conditions [36]. Orgill-Hollands model, on the other hand, is widely utilized for GHI decomposition in the performance models [9], [11], [12] but other approaches, such as Erbs model, are also used [8], [33]. Transposition models, such as Hay and Davies [41], Perez [42], Reindl [43], and Isotropic Sky diffuse [44] models, are used to further determine the diffuse irradiance from the sky received by a tilted surface. The choice of the clear sky model also varies depending on the study. Clear sky model refers to the model that predicts solar irradiance under cloudless sky. Perez model is reported to have a considerably good accuracy [34], [45] and it is utilized in numerous studies, including Yusufoglu et al. [32],

Khan et al. [11], Rodríguez-Gallegos et al. [34], and Sun et al. [12]. Extensive evaluation of decomposition models implemented by Gueymard and Ruiz-Arias [46] also highlights the accuracy of Perez family models. A worldwide validation performed by Yang [47] agrees with aforementioned studies and reports that the Perez family models are among the most accurate models. However, the decomposition and transposition models are sensitive to errors and, for instance, at high latitudes the models can perform somewhat differently, for example, due to high occurrence of low sun elevation angles [36]. Manni et al. [36] studied the performance of 29 decomposition and 25 transposition models and their 725 combinations at Nordic latitudes. Their findings showed that, for instance, Orgill-hollands model did not perform particularly well compared to many other models [36]. However, Perez family models were once again included among the best performing models. Furthermore, some models, such as Erbs model, which were classified by Gueymard and Ruiz-Arias as low performing models were found to perform best at high latitudes [36].

Moreover, the reflected irradiance is studied in varying degrees in the BPV performance models. In particular, there are differences in considering the self-shading of the panel. Self-shading refers to the situation where the PV panel blocks the GHI from entering behind it. When the module casts a shadow on the ground, the reflectivity of the shaded and unshaded ground is non-uniform and, thus, the irradiance reflected from the ground is anisotropic [45]. In some models the ground reflected irradiance is considered anisotropic [10], [12] whereas some models assume that the shading is uniform over the panel i.e., ground reflected irradiance is isotropic [9], [32]. In general, irradiance is one of the most important parameters contributing to the temperature and performance of the solar modules because its availability limits both the heat and power generation of PV system [48]. Therefore, the components of solar radiation are further discussed in Section 3.2. Additionally, the calculations for determining the plane of array (POA) irradiance received by the PV panel are presented.

In the PV performance models, the effect of module temperature on the efficiency of module is taken into account by semi-empirical PV module temperature models [9], [11], [12], [13], [33], [34] and by physical device models [10], [35]. However, the semi-empirical models are most commonly used because they allow to predict the module temperature directly from the ambient conditions [49], [50]. These models are considered semi-empirical because they often rely on energy balance and heat transfer equations but the experimental data is needed to tune the model parameters [50], [51]. Of semi-empirical temperature models Sandia [49], Faiman [50], Mattei [51], and TRNSYS [52], [53], [54] models will be covered in this thesis. More detailed

description of these temperature models is found in Section 3.3. These four models were selected for closer inspection because they have been used as a part of several performance models of BPV panels [9], [11], [12], [13]. The semi-empirical models are interesting from the performance modeling point of view since they are computationally efficient, and only the easily accessible meteorological data is needed to determine the module temperature in most cases [49], [50]. The direct prediction of module temperature from the ambient conditions is possible because the information about the material and system-dependent characteristics of the module is included in the model parameters [49]. The model parameters are module-type-specific, and the mounting configuration can also affect the parameters [49].

A noteworthy detail regarding the semi-empirical temperature models is that they are designed for traditional monofacial modules [14]. However, they are also applied to performance models of BPV. For example, Patel et al. [9] used Sandia model in their BPV performance model to estimate the module operating temperature, and consequently, the effect of temperature on the module efficiency. Similarly, Sun et al. [12] and Khan et al. [11] utilized Faiman and TRNSYS (in [11] named Skoplaki) models in their opto-electro-thermal performance models, respectively. Furthermore, Sun et al. [12] stated that in their performance model the Faiman model parameters are calibrated to the nominal operating temperature (NOCT) of bifacial module; however, the parameter values were not reported. Additionally, Khan et al. [11] reported TRNSYS model parameter for bifacial modules that was calculated based on the experimental data of Patel et al. [9]. Since temperature models that are initially designed for monofacial modules are also used to predict the temperature of bifacial modules, it is important to ensure that the model parameters are suitable for bifacial panels as well. There are some studies that compare the accuracy of Sandia and Faiman model estimations when using the model parameters of MPV panels for BPV panel [13], [14]. The study by Riley et al. [13] claims that Sandia model is descriptive also in the case of bifacial panels. On the contrary, Mannino et al. [14] stated that the accuracy of BPV panel temperature estimation was lower with parameters initially determined for MPV panels than with the parameters optimized for BPV panels. Nevertheless, there is still more to investigate. For instance, studies that compare the accuracy of temperature estimations, when using parameters determined for both MPV and BPV panels, have not been found for Mattei and TRNSYS models.

For bifacial panels, there are only a few physical device thermal models described in literature [27], [30], [31]. Zhang et al. [27], Aly et al. [31], and Tina et al. [30] proposed models specifically designed for thermal modeling of BPV. Additionally, Gu et al. [10] and

Shahverdian et al. [35] integrated the physics-based thermal model into the PV performance model to consider the effect of operating temperature on efficiency. The physical device models differ from the previously mentioned semi-empirical models in a way that the physical properties of the module are explicitly included in the model. On the other words, the heat generation and transfer, and material properties are defined in the model to determine the module operating temperature [27], [30], [31]. These types of models allow to study the module temperature in various installation configurations, albedo conditions, and geographical locations. Additionally, the effect of different materials on the module temperature can be studied. One of the main challenges with physics-based thermal models is the higher computational costs in comparison, for instance, with semi-empirical models. However, the advantage is that the study of various scenarios is possible because, as mentioned, the physics of the module are included in the model, and thus the study is not limited to the available measurement data. One aim of this thesis is to build a physics-based thermal model for bifacial PV modules. The methodology for building the model is presented in Section 4.

3.2 Irradiance models

Solar radiation consists of three main components which are direct, diffused and reflected [48]. The radiation components are illustrated in Figure 3. DNI refers to the irradiance that reaches the surface that is perpendicular to the rays coming straight from the direction of the sun without scattering by the particles in the atmosphere [48]. DHI is the scattered component of solar radiation that is received by a horizontal surface [48]. Reflected irradiance, as the name implies, is the component of solar radiation that is reflected from the surface of the earth [48]. When measuring the irradiance received by some system, for instance solar panel, the reflected irradiance can also refer to the solar radiation that is reflected from the surroundings of that system. The total irradiance received by a horizontal surface, namely GHI, is the sum of DNI and DHI as shown in Eq. (1).

$$\mathrm{GHI} = \mathrm{DNI}\cos\theta_Z + \mathrm{DHI}, \quad (1)$$

where θ_Z is the sun zenith angle.

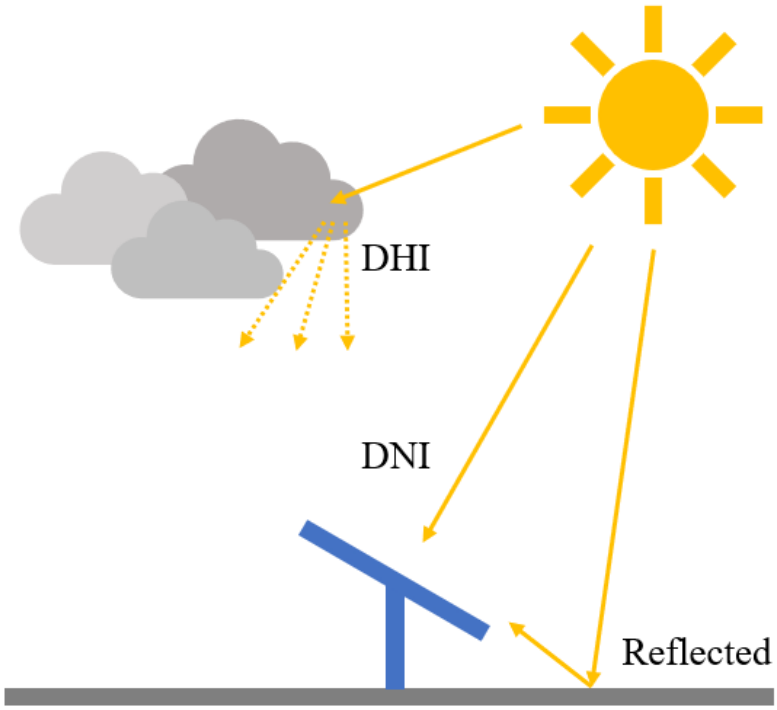

Figure 3: Components of solar radiation.

Furthermore, the total irradiance received by the surfaces of solar panel i.e., the plane of array irradiance (G_{POA}), is the sum of the beam, diffuse, and ground-reflected irradiance components (Eq. (2)) [45].

$$G_{\mathrm{POA}} = G_{\mathrm{b}} + G_{\mathrm{d}} + G_{\mathrm{r}}\,, (2)$$

where G_{b}, G_{d}, and G_{r} are the beam, diffuse, and ground-reflected irradiance, respectively.

The beam irradiance depends on the DNI and the angle of incidence (AOI) according to Eq. (3) [45], [55]. If DNI is unknown, it can be presented as a function of GHI, DNI, and sun zenith angle by solving it from Eq. (1).

$$G_{\mathrm{b}} = \mathrm{DNI}\cos(\mathrm{AOI}) = \frac{(\mathrm{GHI} - \mathrm{DHI})\cos(\mathrm{AOI})}{\cos(\theta_Z)}, (3)$$

Furthermore, in this thesis AOI is the angle between the sun's rays and the normal of the PV panel surface. Therefore, AOI is determined as follows [56]:

$$\mathrm{AOI} = \cos^{-1}[\cos(\theta_{\mathrm{Z}})\cos(\theta_{\mathrm{T}}) + \sin(\theta_{\mathrm{Z}})\sin(\theta_{\mathrm{T}})\cos(\theta_{\mathrm{A}} - \theta_{\mathrm{A,PV}})],\ (4)$$

where θ_T and $\theta_{A,PV}$ are the tilt and azimuth angles of the panel, and θ_A is the azimuth angle of sun. When calculating the irradiance at the rear surface, the θ_{T} is replaced with $\theta_{\mathrm{T}} - 180°$.

As mentioned, there are multiple transposition models that are used for calculating the diffuse horizontal irradiance. The Perez transposition model is presented in more detail, since it is one of the most accurate models in terms of describing the anisotropic G_{d} [34], [45]. The high accuracy is due to complex model that takes into account isotropic, circumsolar, and horizon brightening diffuse components using a set of empirical coefficients for each term [57]. The Eq. (5) shows G_d on the front surface of the panel, according to Perez [42], [58]. For G_d at the rear surface, the tilt angle is $\theta_{\mathrm{T}} - 180°$.

$$G_d = \mathrm{DHI}\left[(1 - F_1)\left(\frac{1 + \cos(\theta_{\mathrm{T}})}{2}\right) + F_1\left(\frac{a}{b}\right) + F_2 \sin(\theta_{\mathrm{T}})\right], (5)$$

where F_1 and F_2 are coefficients expressing the degree of circumsolar and horizon anisotropy, given in literature [58]. Furthermore, parameters a and b are defined as follows [58]:

$$a = \max(0, \cos(\mathrm{AOI})), \ (6)$$

$$b = \max\left(\cos(85°), \cos(\theta_{\mathrm{Z}})\right), (7)$$

The isotropic ground reflected irradiance received by the surface depends on albedo along with GHI and tilt angle of the surface as shown in Eq. (8) [45].

$$G_{\mathrm{r}} = \mathrm{GHI}\ \rho\ \frac{1 - \cos\theta_{\mathrm{T}}}{2}, (8)$$

where ρ is the albedo, and $\frac{1-\cos\theta_{\mathrm{T}}}{2}$ is the ground view factor. For G_{r} at the rear surface, the tilt angle is $\theta_{\mathrm{T}} - 180°$.

In Eq. (8), as is usually the case with isotropic models, the shaded ground view factor is assumed to be zero. Conversely, in the anisotropic models the view factor from shaded ground is included [45]. Generally, the anisotropic ground reflected irradiance can be calculated as follows [45]:

$$G_{\mathrm{r}} = \rho\ F_{\mathrm{m\rightarrow usgrd}}\ \mathrm{GHI} + \ \rho\ F_{\mathrm{m\rightarrow sgrd}}\ \mathrm{DHI}, (9)$$

where $F_{\mathrm{m\rightarrow usgrd}}$ and $F_{\mathrm{m\rightarrow sgrd}}$ are view factors of unshaded and shaded grounds, respectively.

The modeling of anisotropic behavior of ground reflected irradiance is considered challenging but it is also significant for the accurate performance estimation of solar modules [45]. Accurate models for the ground reflected irradiance are especially important for bifacial PV since the G_{r}

may account for a significant portion of the total irradiance entering the surfaces of the panel, depending on the mounting configuration [16]. In addition to the shading conditions, another important factor affecting the G_r is the reflectivity of the ground i.e., albedo [16]. The albedo varies for different materials depending on their surface properties [4]. Table 2 collects the albedo values of materials that can be found in the solar panel installation environments. The albedo value is defined as a ratio of horizontal reflected irradiance (HRI) and GHI [4].

Table 2: Albedo values of common ground materials

Ground material	**Albedo** [4]
Brick	0.3
Wood	0.15
Corrugated iron	0.13
Concrete	0.225
Snow (fresh)	0.8–0.88
Snow (2–5 day old)	0.75–0.8
Grass	0.205
Urban environment	0.18 [59]

3.3 Photovoltaic module temperature models

3.3.1 Sandia

Empirical Sandia module temperature model is developed at Sandia National Laboratories for the purposes of the performance modeling [49]. Sandia model has proven to be adequate to its purposes since it provides the estimation about the operating temperature of module with an accuracy of ± 5°C. The variation of this magnitude in the module temperature causes error of 3 % at the highest when modelling the power production of the module [49]. However, in terms of the temperature estimation alone, variation of ± 5°C can already be considered notable.

The Sandia model predicts the module temperature according to Eq. (10). Moreover, the model parameters can be determined by fitting the linearized form of Sandia model to the experimental or modeled data according to Eq. (11) [49].

$$T_{\mathrm{m}} = T_{\mathrm{amb}} + G(e^{bv+a}), (10)$$

$$\log\left[\frac{T_{\mathrm{m}} - T_{\mathrm{amb}}}{G}\right] = bv + a, (11)$$

where T_m and T_{amb} are the module temperature and ambient temperature, respectively, G is total irradiance received by the module (POA irradiance), v is the windspeed and a and b are the module-type-specific model parameters. For bifacial panels $G = G_f + G_r$ i.e., the sum of front and rear irradiance.

In Sandia model, the model parameter a is the intercept coefficient, and b is the slope of the linear fit. The parameter a defines the upper limit of the module temperature at low wind speeds while b describes the decrease rate of the module temperature as the wind speed increases. With the information included in model parameters, it is possible to predict the module temperature as a function of the ambient temperature, solar irradiance, and wind speed.

3.3.2 Faiman

Faiman module temperature model is modified from Hottel-Whiller-Bliss (HWB) equation (Eq. (12)) that is developed for studying the flat-plate solar-thermal collectors under steady state conditions [50]. The HWB equation can be applied to PV solar modules because in Faiman model the thermal mass of the module is assumed to have a negligible effect on the heat exchange with the environment [50].

$$\eta = \eta_0 - \frac{U}{G}(T_{\mathrm{m}} - T_{\mathrm{amb}}), (12)$$

where η is the efficiency of solar-thermal collector, η_0 is the optical part of efficiency, and U is the heat transfer coefficient.

To adapt HWB model for solar modules it is assumed that solar-thermal collector could produce electrical power in addition to thermal power. Eq. (13) describes the amount of thermal power that could be extracted from collector that also produces electrical power [50].

$$G\eta = G\eta_0 - U(T_{\mathrm{m}} - T_{\mathrm{amb}}) - G\eta_{\mathrm{e}}, (13)$$

where η_{e} is the electrical efficiency.

Furthermore, when thermal power that could be used decreases to zero, the η also decreases to zero [50]. Consequently, the maximum temperature of thermal-collector is reached and Eq. (12) can be presented as follows:

$$T_{\mathrm{max}} = T_{\mathrm{amb}} + \frac{G(\eta_0 - \eta_{\mathrm{e}})}{U}, (14)$$

To study the effect of wind speed on module temperature U is parametrized as $U_{\mathrm{L1}}v + U_{\mathrm{L0}}$,

where $U_{\mathrm{L0}} = \frac{U'_{\mathrm{L0}}}{\eta_0 - \eta_{\mathrm{e}}}$ and $U_{\mathrm{L1}} = \frac{U'_{\mathrm{L1}}}{\eta_0 - \eta_{\mathrm{e}}}$.

With these modifications HWB model (Eq. (12)) takes a form that is known as Faiman module temperature model (Eq. (15)) [50]. The linearized Faiman model is shown in Eq. (16).

$$T_{\mathrm{m}} = T_{\mathrm{amb}} + \frac{G}{U_{\mathrm{L1}}v + U_{\mathrm{L0}}}, (15)$$

$$\frac{G}{T_{\mathrm{m}} - T_{\mathrm{amb}}} = U_{\mathrm{L1}}v + U_{\mathrm{L0}}, (16)$$

U_{L0} and U_{L1} are the Faiman model parameters that must be determined in order to estimate module temperatures based on the meteorological data. The parameters are provided by applying the linear model into a data that describes the module temperature as a function of irradiance, ambient temperature and wind speed. The intercept coefficient of the fitted line (U_{L0}) describes the effect of solar irradiation and the slope (U_{L1}) describes the effect of wind speed on the module temperature [50] For bifacial panels $G = G_f + G_r$.

3.3.3 Mattei

Mattei model is experimentally validated model that allows the study of module temperature against the irradiance, ambient temperature and wind speed [51]. The model neglects the radiative heat transfer and assumes that the temperature is uniform across the module and there is no temperature difference between cells and the cover glass. However, the modeling results are claimed to be in good agreement with the experimental data [51].

Mattei model defines the temperature by Eq. (17) [51]. The linearized form of the model is shown in Eq. (18).

$$T_{\mathrm{m}} = \frac{U_{\mathrm{PV}}T_{\mathrm{amb}} + G[\alpha_{\mathrm{tot}} - \mathrm{PCE}_{\mathrm{ref}} - \beta \mathrm{PCE}_{\mathrm{ref}} T_{\mathrm{ref}}]}{U_{\mathrm{PV}} - \beta \eta_{\mathrm{ref}} G}, (17)$$

$$U_{\mathrm{PV}} = \frac{G[\alpha_{\mathrm{tot}} - \mathrm{PCE}_{\mathrm{ref}} - \beta \mathrm{PCE}_{\mathrm{ref}} (T_{\mathrm{m}} - T_{\mathrm{ref}})]}{(T_{\mathrm{m}} - T_{\mathrm{amb}})}, (18)$$

where α_{tot} is the total absorption coefficient, $\mathrm{PCE}_{\mathrm{ref}}$ is the efficiency at reference temperature ($T_{\mathrm{ref}} = 25°\mathrm{C}$), and β is the temperature coefficient of cell and U_{PV} is the Mattei model parameter. For bifacial panels $G = G_f + G_r$.

The parameter U_{PV} refers to the overall convective heat transfer of the panel, and it can be parameterized as $U_{\mathrm{PV1}}v + U_{\mathrm{PV0}}$ [51]. In other words, U_{PV} is the sum of the convective heat transfer coefficients (h) on the front and rear surfaces of the module. Therefore, the differences in the parameter U_{PV} mainly arise from the differences in the convective heat transfer of the modules [51]. It is noteworthy, that unlike in Sandia and Faiman models, the information about the characteristics of the module is included in other variables than the model parameter U_{PV}. In this model, the material properties of the module, such as absorption, efficiency, and temperature coefficient, are specified in the parameters α_{tot}, $\mathrm{PCE}_{\mathrm{ref}}$, and β.

3.3.4 TRNSYS

Like the other models mentioned, TRNSYS model is semi-empirical model which means that the model parameter is determined using the experimental data [53]. This model neglects the radiative heat transfer and free-convection. It is stated that excluding the radiative heat transfer and free-convection leads to error less than 2°C when the wind speed higher than 0.2 m/s [53].

The TRNSYS model estimates the module temperature based on Eq. (19) [52], [53], [54]. The model parameter is determined by fitting linearized TRNSYS to simulated temperature data model shown in Eq. (20).

$$T_{\mathrm{m}} = T_{\mathrm{amb}} + \alpha_{\mathrm{tot}} \frac{G}{U_{\mathrm{Loss}}} \left[1 - \frac{\mathrm{PCE}_{\mathrm{ref}}}{\alpha_{\mathrm{tot}}}\right], (19)$$

$$U_{\mathrm{Loss}} = \frac{\alpha_{\mathrm{tot}} G \left[1 - \frac{\mathrm{PCE}_{\mathrm{ref}}}{\alpha_{\mathrm{tot}}}\right]}{(T_{\mathrm{m}} - T_{\mathrm{amb}})}, (20)$$

where U_{Loss} is TRNSYS model parameter. For bifacial panels $G = G_f + G_r$.

The parameter U_{Loss} describe the overall thermal loss coefficient [52], [53], [54]. Since the radiative heat transfer and free-convection are ignored, U_{Loss} include the information about the overall convective heat transfer of the module. To plot $(\alpha_{\mathrm{tot}} G \left[1 - \frac{\mathrm{PCE}_{\mathrm{ref}}}{\alpha_{\mathrm{tot}}}\right])/(T_{\mathrm{m}} - T_{\mathrm{amb}})$ as a function of wind speed, the U_{Loss} is parameterized as $U_{\mathrm{Loss1}}\, v + U_{\mathrm{Loss0}}$. Similar to Mattei model, this model considers the characteristics of materials and system in parameters other than U_{L}, that is α_{tot} and $\mathrm{PCE}_{\mathrm{ref}}$.

4 Modeling work – Thermal model of mono- and bifacial photovoltaic panels

4.1 Model geometry and Materials

In this thesis, a three-dimension (3D) thermal model of mono- and bifacial silicon PV module was built with COMSOL Multiphysics that is a finite element modeling (FEM) software, similarly as presented in Varjopuro et al. [60]. The geometry of MPV and BPV modules are identical. Both modules consist of front and rear glasses, ethylvinylacetate (EVA) layers, and silicon solar cells as presented in Figure 4. Silicon cells with the dimensions of 15.6 cm times 15.6 cm are placed between two EVA layers. The silicon cells in the modeled MPV and BPV panels correspond to the mono-PERC and PERT cells described in Section 2.1, respectively. The modeled panels have 72 cells in six rows, and the distance between the adjacent cells is 1 cm. Therefore, the dimensions of the whole panel are 200.2 cm times 100.6 cm. The front and rear glasses are both 3 mm thick while EVA layers are 0.5 mm thick. The silicon cells were modeled as a thin film layer to simplify the mesh, and thus, to decrease the computation time.

In addition to model geometry, the thermal conductivity (K), density (ρ), and specific heat capacity (c_p) of the panel components should be specified. The specific heat capacity along with the density determines the amount of energy that is needed to change the temperature of a panel component by one degree. The thermal conductivity in turn specifies the ability of material to conduct heat. Table 3 concludes the material properties of glass, EVA and silicon and the thicknesses of glass and EVA.

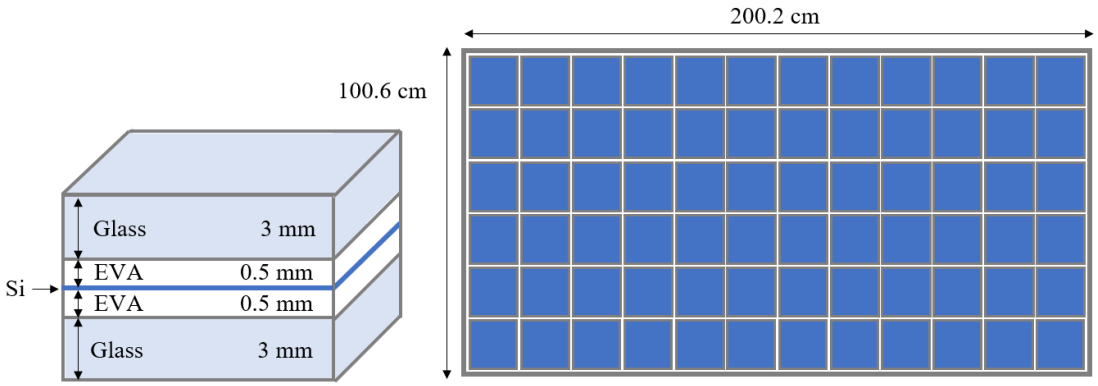

Figure 4: Components of the silicon solar cell (left) and design of the panel (right).

Table 3: Material properties and thicknesses of the components of silicon solar module from [61]

	Glass	EVA	Silicon
K [W/(mK)]	2	0.311	130
ρ [kg/m^3]	2450	950	2330
c_p [J/(kgK)]	500	2090	677
D [mm]	3	0.5	-

4.2 Heat transfer

The thermal energy is transferred from the module to the ambient by three main mechanisms that are conduction, convection, and radiative heat transfer [62]. Fourier's law of heat conduction (Eq. (21)) and heat equation (Eq. (22)) define the rate of heat flow through the material [62].

$$\vec{q} = -K\nabla \mathrm{T}, (21)$$

$$\mathrm{Q} + K\nabla^2 \mathrm{T} = 0, (22)$$

Convective heat flux describes the heat transfer through the air flow. Here the convective heat flux was applied to all outermost surfaces of the panel. The convective heat transfer was defined according to Eq. (23) that excludes the radiation term [63].

$$-\vec{n} \cdot \vec{q} = h(T_{\mathrm{amb}} - T_{\mathrm{m}}), (23)$$

where $\vec{q}$ is the convective heat flux, h is the convective heat transfer coefficient, T_{amb} is the ambient temperature, and T_m is the module surface temperature.

The convective heat transfer coefficient depends on the wind speed as follows [64]:

$$h = 2.8\frac{\mathrm{W}}{\mathrm{m^2K}} + 3\frac{\mathrm{Ws}}{\mathrm{m^3K}}v, (24)$$

In the literature, there are multiple options for the heat transfer coefficient, and the choice of the suitable coefficient is affected by, for instance, the tilt angle of the module [65], [66]. On the rear side of the tilted panel, the convective heat transfer coefficient was presumed to be half to that on the front surface [65], [67]. In the case of vertical panels, h was determined to be equal on both sides.

Heat transfer through the radiation does not require the medium to transfer heat [63]. Here the radiative heat transfer occurs between the panel and its surroundings. The radiative heat transfer is determined as Eq. (25) show [63].

$$-\vec{n} \cdot \vec{q} = \varepsilon\sigma(T_{\mathrm{amb}}^4 - T_{\mathrm{m}}^4), (25)$$

where ε = 0.85 is the surface emissivity and σ is the Stefan−Boltzmann constant ($5.67 \cdot 10^{-8}$ $W/m^{-2}K^{-4}$)

4.3 Heat generation

The solar panel converts incoming radiation into electricity. The portion of absorbed irradiance that is not converted into electricity turns into heat energy. This excess heat energy leads to an increase in the temperature of the panel. In this model, the heat generation was described according to Eq. (26) correspondingly as in the study by Varjopuro et al. [60]. In the case of bifacial panels, the overall heat generation is the sum of heat generated based on the irradiance received by the front and rear surfaces of the panel. The model parameters for calculating the heat generation are described in Table 4.

$$Q(G, T_{\mathrm{cell}}) = \frac{\big(1 - \eta_{\mathrm{e}}(G, T_{\mathrm{cell}})\big)\alpha_{\mathrm{tot}}(T_{\mathrm{cell}})G}{D_{\mathrm{cell}}}, (26)$$

where T_{cell} and D_{cell} are the temperature and thickness of the cell, respectively.

Both η_{e}, and α_{tot} depend on temperature which is due to temperature dependance of band gap. The temperature induced effect on the band gap for silicon is −0.273 meV/K [68]. The band gap of silicon narrows as the temperature rises which leads to higher thermalization and, thus, heat generation [69]. The changes in the band gap energy also affect the open circuit voltage of system, and furthermore efficiency [69]. At the irradiance of 1000 W/m^2 and temperature of 25°C i.e., at the reference irradiance (G_{ref}) and temperature (T_{ref}), the reference power conversion efficiency ($\mathrm{PCE}_{\mathrm{ref}}$) was determined to be 20 % for the monofacial panel and front side of the bifacial panel. $\mathrm{PCE}_{\mathrm{ref}}$ for the rear side of the bifacial panel was set to 18 %. The bifaciality of the PV technology is determined by the ratio of the power production of the front and rear surfaces [13]. In this model, the bifaciality of the panel was taken into account by setting a different value for the efficiency of the front and rear surfaces. When the temperature differs from reference conditions, electrical efficiency was defined according to Eq. (27).

$$\eta_{\mathrm{e}}(G, T_{\mathrm{cell}}) = \frac{\mathrm{PCE}(G, T_{\mathrm{cell}})}{\alpha_{\mathrm{tot}}(T_{\mathrm{cell}})}, (27)$$

where power conversion efficiency (Eq. (28)) [60] and total absorption (Eq. (29)) at G and T_{cell} are

$$\mathrm{PCE}(G, T_{cell}) = \mathrm{PCE}_{\mathrm{ref}}\left[1 + \frac{n k_{\mathrm{B}} T_{\mathrm{ref}}}{V_{\mathrm{OC,ref}}\, q} \ln\left(\frac{G}{G_{\mathrm{ref}}}\right)\right]\left(1 + \beta(T_{\mathrm{cell}} - T_{\mathrm{ref}})\right), (28)$$

and

$$\alpha_{\mathrm{tot}}(T_{\mathrm{cell}}) = \frac{\int_{300\ \mathrm{nm}}^{\lambda_{\mathrm{E_g}(T_{\mathrm{cell}})}} \boldsymbol{\alpha}(\lambda < \boldsymbol{\lambda}_{\mathrm{E_g}})\, G_\lambda\, d\boldsymbol{\lambda} + \int_{\lambda_{\mathrm{E_g}(T_{\mathrm{cell}})}}^{4000\ \mathrm{nm}} \alpha(\lambda \geq \lambda_{\mathrm{E_g}})\, G_\lambda\, d\boldsymbol{\lambda}}{\int_{300\ \mathrm{nm}}^{4000\ \mathrm{nm}} G_\lambda \quad d\boldsymbol{\lambda}}, (29)$$

in which n is the ideality factor, k_{B} is the Boltzmann constant, $V_{\mathrm{OC,ref}}$ is the open circuit voltage of the cell at G_{ref} and T_{ref}, q is the elementary charge, β is the temperature coefficient of efficiency, G_λ is the solar irradiance spectrum, $\lambda_{\mathrm{E_g}}$ is the maximum wavelength absorbed by the semiconductor material at T_{cell}, and $\alpha(\lambda < \lambda_{\mathrm{E_g}})$ and $\alpha(\lambda \geq \lambda_{\mathrm{E_g}})$ are above and below band gap absorption, respectively.

Table 4: Model parameters for calculating the heat generation

Model Parameter	**MPV | BPV**
$\mathbf{PCE_{ref,front}}$	20 | 20 %
$\mathbf{PCE_{ref,rear}}$	0 | 18 %
$\boldsymbol{E_g(T = 25\ °C)}$	1.12 eV [70]
$\boldsymbol{\beta_{E_g}}$	-0.273 meV/K [68]
$\boldsymbol{\beta_T}$	-0.35 %/K [71]
$\boldsymbol{n}$	1.3 [72], [73]
$\boldsymbol{V_{OC,ref}}$	0.6 V [72], [73]
$\boldsymbol{\alpha(\lambda < \lambda_{E_g})}$	0.95 [74]
$\boldsymbol{\alpha(\lambda \geq \lambda_{E_g})}$	0.2 [74]

4.4 Irradiance model

Irradiance is a relevant component of the temperature models. Here the total irradiance received by the bifacial panel (POA) was calculated using the Purdue Bifacial irradiance model provided by Sandia's PVLIB [75]. The model allowed to simulate direct, diffuse, and ground reflected irradiance on both surfaces of tilted and vertical BPV panels. Total irradiance received by the monofacial panel was modeled using the same methods, but the irradiance received by the back surface was ignored. When modeling the POA irradiance, it was assumed that both mono- and bifacial panels are mounted on a flat roof so that the bottom edge of the panel touches the roof, as Figure 5 shows. The albedo of the roof was set to 0.18 which is a typical albedo value for an urban environment.

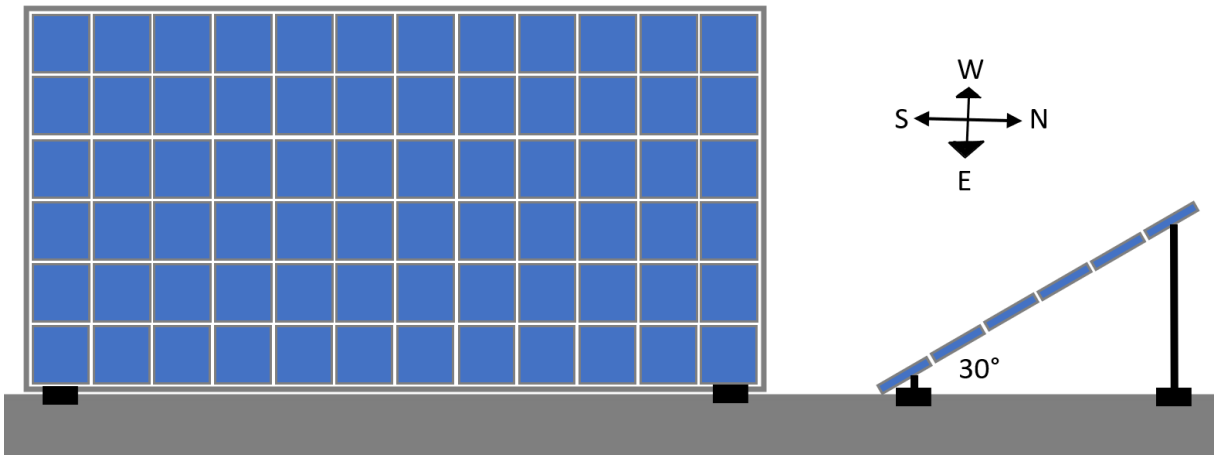

Figure 5: Installation configuration of the vertical BPV panel (left), and the tilted MPV and BPV panels (right).

In the present irradiance model, the sun zenith and azimuth angles were determined based on time and location, including latitude, longitude and elevation of measurement site. This feature would allow us to study the total irradiance, and thus also, the temperature of the panel in varying locations. Furthermore, the angle-of-incidence was determined for all sun zenith and azimuth angles of a given location according to Eq. (4). The reflection losses at the interface of the glass and air were taken into account by angular reflection losses equation developed by Martin and Ruiz [76], [77]. GHI was decomposed into DNI and DHI using the DIRINT model.

Once the required input values (DNI, DHI, AOI) were solved, G_{b}, G_{d}, and G_{r}, and finally, the G_{POA} could be calculated. In this model, the direct irradiance (G_{b}) was calculated as Eq. (3) shows and the diffuse irradiance from the sky (G_{d}) by the Perez transposition model (Eq. (5)). The irradiance reflected from the ground (G_{r}) was determined by using a model that fully

accounts for the self-shading losses by applying view-factor model presented by Sun et al. [12]. On the other words, in the ground reflected irradiance calculations, it was considered that PV system prevents the direct and circumsolar diffuse light and the isotropic diffuse light from entering the ground. In such case, the shading of the ground is non-uniform. The area of the shaded ground depends on the solar position and panel mounting. The sum of G_{b}, G_{d}, and G_{r} of both front and rear surfaces compose the total irradiance received by a panel (G_{POA}). This calculated POA irradiance was set as an input value in the thermal model.

4.5 Model validation

To ensure the accuracy of the thermal and irradiance model described above, model validation was performed. The in-situ data from vertically mounted bifacial panels at the measurement site of Turku University of Applied Sciences (TUAS) in Turku was utilized for validating the bifacial thermal model and the irradiance model. The monofacial thermal model was, in turn, validated with the in-situ data collected from the tilted monofacial panels installed on the measurement site of Finnish Meteorological Institute (FMI) in Helsinki. The specifications of both PV systems are shown in Table 4.

Table 5: The specifications of PV systems

PV system	Bifacial	Monofacial
Location	Turku (60°N, 22°E)	Helsinki (60°N, 25°E)
PV panel	Prism Solar model Bi60-375BSTC	SolarWorld Protect SW 250 poly
Installation	Vertical	Floating on flat roof
Tilt angle	90°	15°
Azimuth angle	90°	135°
Commission date	18/08/2017	24/08/2015
Efficiency [%]	17.7 / 15.9	14.9
Temperature coefficient [%/°C]	–0.4139	-0.41

For both mono- and bifacial panels the POA irradiance, GHI, ambient temperature, and panel temperature were available in minute resolution. The temperature of bifacial panel was recorded from the front surface while the temperature of monofacial panel was measured from the back surface inside the insulated capsules. The wind speed was recorded minute by minute at TUAS' site and every 10 minutes at FMI's site. When minute resolution data was not available, the data was interpolated.

4.5.1 Data filtering

The quality and accuracy of the collected GHI data as well as the calculated DNI and DHI values, was assured by applying multiple filters to the data. The unrealistic values were filtered using the following conditions introduced by Gueymard and Ruiz-Arias [46]:

1. $\mathrm{GHI} > 0, \mathrm{DHI} > 0, \mathrm{DNI} \geq 0$
2. $\theta_Z < 85°$
3. $\mathrm{DNI} < G_0$
4. $\mathrm{DNI} < 1100 + 0.03\ \mathrm{El}$
5. $\mathrm{DHI} < 0.95\ G_0 \cos^{1.2}(\theta_Z) + 50$
6. $\mathrm{GHI} < 1.5\ G_0 \cos^{1.2}(\theta_Z) + 100$
7. $|100\ (\mathrm{DNI}\cos(\theta_Z) + \mathrm{DHI} - \mathrm{GHI})/\mathrm{GHI})| < 5\%$
8. $\frac{\mathrm{DHI}}{\mathrm{GHI}} < 1.05$ for $\mathrm{GHI} > 50, \theta_Z < 75°$
9. $\frac{\mathrm{DHI}}{\mathrm{GHI}} < 1.10$ for $\mathrm{GHI} > 50, \theta_Z > 75°$

where El is the surface elevation, and G_0 is the extraterrestrial irradiance on a normal surface.

Conditions 1 and 2 were used to remove the datapoints measured during night hours and the low solar elevation angles i.e., the irradiance values measured close to sunrise and sunset. Conditions 4-6 were applied to define the theoretical maximum values for the irradiance components. For instance, DNI cannot exceed extraterrestrial irradiance which equals to the irradiance received by the horizontal surface at the top of the atmosphere (Condition 3). Condition 7 was used to check that the sum of DNI and DHI equals to GHI with the tolerance of 5 percent. Conditions 8 and 9 were applied to ensure that DHI does not exceed the GHI. Condition 8 was applied when the sun zenith angles were below 75° whereas Condition 9 was applied when the sun zenith angles were above 75°. Theoretical limit for the ratio of DHI to GHI is 1.0 but tolerances of 5 and 10 percent were included in the Conditions 8 and 9, respectively.

In addition to filters described above, the snow filter was applied to the monofacial PV dataset because it included information about the snow depth in the ground. The periods during which the depth of the snow on the ground was greater than zero were removed from the dataset of monofacial panel. It can be assumed that when there was no snow on the ground, there was also no snow on the surface of the panel. Similar methods for filtering out the periods during which the panels are covered in snow are described in the literature [59], [78]. The information about snow conditions was not included in the bifacial PV dataset. However, it would be unlikely that

the snow would cover the surface of the vertical panel and, thus, it was assumed that the snow did not disturb the irradiance measurement.

Finally, the rapid variations of measured GHI values were removed. This was done because the present thermal model is a steady-state model which means that the modeled operating temperature does not change over time. Therefore, if the GHI value differed from 10-minute average more than 25 W/m^2, the value was removed.

4.5.2 Irradiance model validation

The choice of decomposition and transposition models directly affects the accuracy of solar irradiance estimation [36]. Inaccuracies of the models can lead to either over- or underestimation of the irradiance received by the surface [36]. Therefore, the performance of the irradiance model used in this thesis was validated. In Figure 6 the calculated POA irradiance is presented as function of the measured POA irradiance. The calculated POA irradiance was defined as described in Section 4.4. The measured POA irradiance data was collected from the front and back surfaces of the vertical PV system at the TUAS's site. The measurement data from TUAS was used for irradiance model validation because the panels are bifacial.

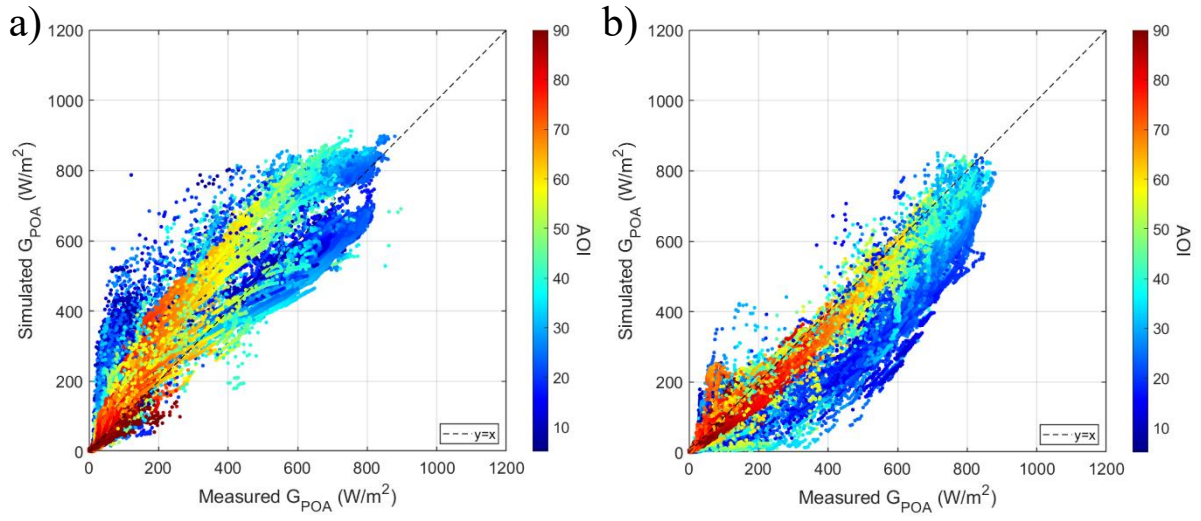

Figure 6: The modeled POA irradiance on the a) front (east facing) and b) rear (west facing) surface of the panel as a function of the measured one.

The DIRINT model combined with the Perez transposition model seems to somewhat overestimate the irradiance received by the east-facing surface but underestimate the irradiance received by the west-facing surface (Figure 6). More accurate model predictions are achieved when the AOI is closer to 90 degrees. The mean absolute error (MAE), root mean squared error

(RMSE), correlation coefficient and bias for modeled POA irradiance of the east- and west-facing surface are shown in Table 6.

Table 6: Evaluation metrics for modeled POA irradiance of the east- and west-facing surface

	MAE [W/m^2]	RMSE [W/m^2]	Corr. Coeff.	Bias [W/m^2]
East-facing	42.0	73.9	0.957	-27.2
West-facing	32.7	59.6	0.972	13.7

Manni et al. [36] reported the 725 combinations of decomposition and transposition models for the east- and west-facing surfaces. They stated that when the same decomposition and transposition models are utilized to model the irradiance received by both east- and west-facing surfaces of the module, the model overestimates the irradiance of one surface and underestimates that of the other surface. In the study by Manni et al. [36], the irradiance models were validated against measurement data from the same vertical PV system at TUAS' rooftop as in this thesis and, therefore, the results are a good reference. The evaluation metrics and the comparison with reported results indicate that the irradiance model used in this thesis works well.

4.5.3 Thermal model validation

Because the available experimental data was collected with 1-minute resolution during several years, the size of the dataset is very large. To save the computational resources, the number of points utilized for model validation had to be limited. A representative set of points was selected by first specifying a set of ambient temperatures, wind speeds and solar irradiances. The aim was that the combinations of selected ambient temperatures, wind speeds and solar irradiances comprehensively describe the realistic operation conditions of solar panels. Thus, the ambient temperatures were selected to range from 5 to 30°C every 5°C. Furthermore, wind speeds from 1 to 10 m/s every 1 m/s and solar irradiances from 100 to 1000 W/m^2 every 100 W/m^2 were selected. The points closest to these specified environmental conditions were included in the validation dataset as presented in Figure 7. The Euclidian norm function, that measures the distance between specified points and the experimental datapoints, was utilized in the point selection. The validation dataset for the thermal model of monofacial (Figure 7a) and bifacial (Figure 7b) panels was created on the same principle from the experimental data of FMI and TUAS, respectively. Figure 7a and Figure 7b shows that the selected datapoints are quite evenly distributed over the different conditions meaning that the different irradiances, wind speeds,

and ambient temperatures are widely represented in the validation datasets. The methods for validating the thermal models are identical with those presented by Varjopuro et al. [60].

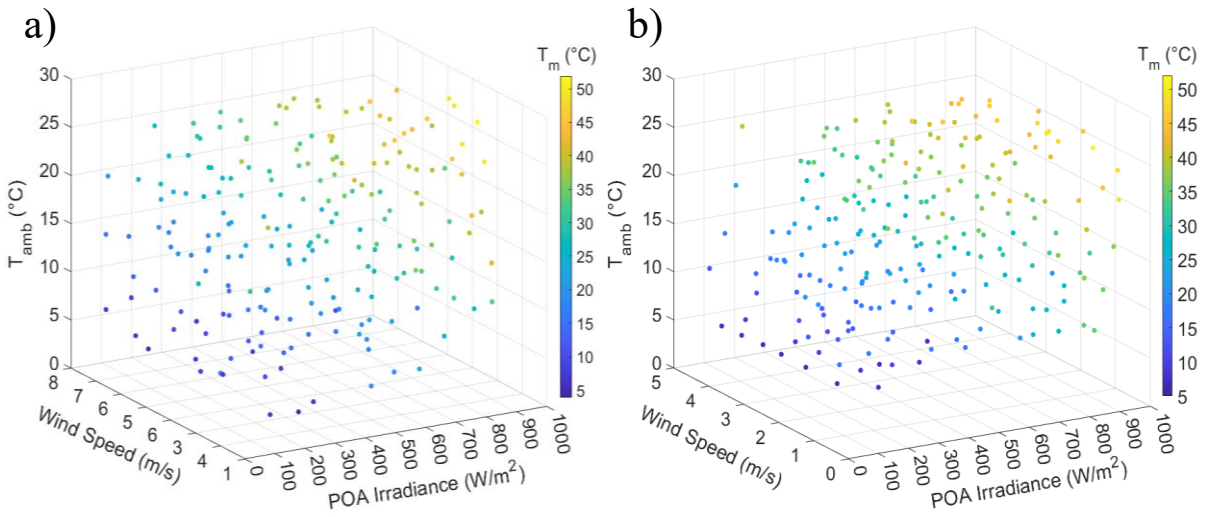

Figure 7: The selection of the datapoints for the validation of thermal models from the experimental data of a) TUAS and b) FMI. The color of the point illustrates the module temperature.

After the representative set of data was selected, the modeled temperature of mono- and bifacial modules was compared to the measured ones as Figure 8 shows. In the case of the monofacial panel, the modeled temperature refers to the highest temperature of the rear surface of the panel whereas in the case of bifacial panel, it refers to the average temperature of the rear surface. This is because in the monofacial panels, the thermocouple is usually placed on the rear surface of the panel at the point corresponding to the center of the cell, which is usually the hottest point. However, in the case of bifacial panels, this cannot be done as there are cells on the rear surface as well. Therefore, in the bifacial panels, the thermocouple must be placed between the cells and, thus, the modeled average temperature of the rear surface better reflects the actual situation. In the case of the vertical PV panels with glass-cell-glass structure it should not affect the results whether the front or rear surface temperature is evaluated because the convection is assumed to be in the same order of magnitude at both sides. However, the wind direction may affect the convective cooling of different surfaces of the panel. The present thermal model does not account the wind direction but it could be considered in the future studies.

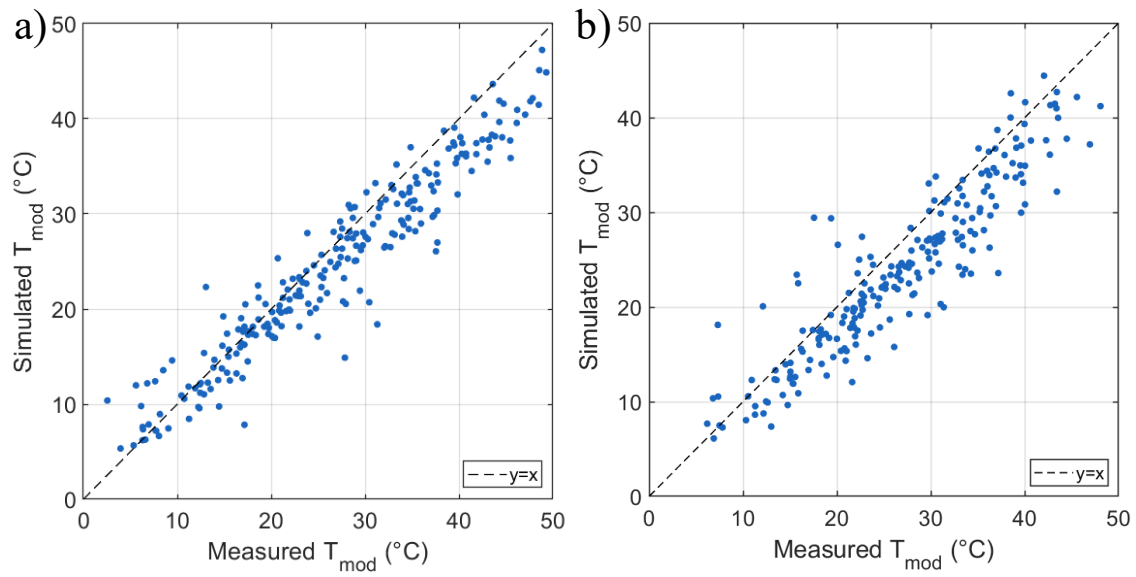

Figure 8: The modeled temperature of a) monofacial and b) bifacial PV panel as a function of the measured one.

When the modeled temperature is presented in relation to the measured temperature, it is seen that the points are well aligned with the dashed line that represent the ideal relationship between the variables (Figure 8). Furthermore, the evaluation metrics, presented in Table 7, indicate that the thermal model predicts the module temperature of mono- and bifacial panel well.

Table 7: Evaluation metrics for the thermal model of the mono- and bifacial panels

	MAE [°C]	**RMSE [°C]**	**Corr. Coeff.**	**Bias [°C]**
Monofacial	3.2	4.0	0.963	2.4
Bifacial	3.6	4.3	0.942	2.9

5 Modeling results

5.1 Comparison of operating temperature of mono- and bifacial panels in varying ambient conditions

To compare the absolute differences in the operating temperatures of mono- and bifacial panels, the steady-state temperature was simulated in varying ambient conditions. The POA irradiances, calculated from specified GHI irradiances (Section 4.4), were set as a model input for irradiance. The effect of ambient temperature, GHI irradiance, and wind speed on the operating temperature of MPV and tilted BPV panels was studied by changing one variable at the time (Figure 9a-8c). The ambient temperature, GHI, and wind speed were 20°C, 800 W/m^2, and 1 m/s, respectively, unless stated otherwise. The POA was calculated from GHI assuming that the position of sun corresponds to its typical position at the noon on the 15th of June in Helsinki (60.20° N, 24.96° E) (Figure 9a and Figure 9b). The temperatures of MPV and BPV panels, with a tilt angle of 30 degree, were directly compared under these specified ambient conditions.

Due to the different tilt and azimuth angles of the PV panels, it was not convenient to compare the operating temperature of vertical BPV panels with that of tilted panels at a specific time. Around noon the sun's rays are almost perpendicular to the front surface of the south facing panel, and thus the irradiance received by the panel is high. On the contrary, around noon the sun's rays hit the vertical panel at a very small angle which leads to significantly lower POA irradiance. For this reason, the operating temperatures of panels with different orientations were not compared at given time of the day but rather during the day, as shown in Figure 9d. The ambient temperature, wind speed and GHI were kept constant, that was 20°C, 1 m/s, and 600 W/m^2 throughout the day. It is essential to highlight that the present thermal model is a steady-state model, which means that the Figure 9d compares the steady-state temperature of the panels at irradiance conditions of different times.

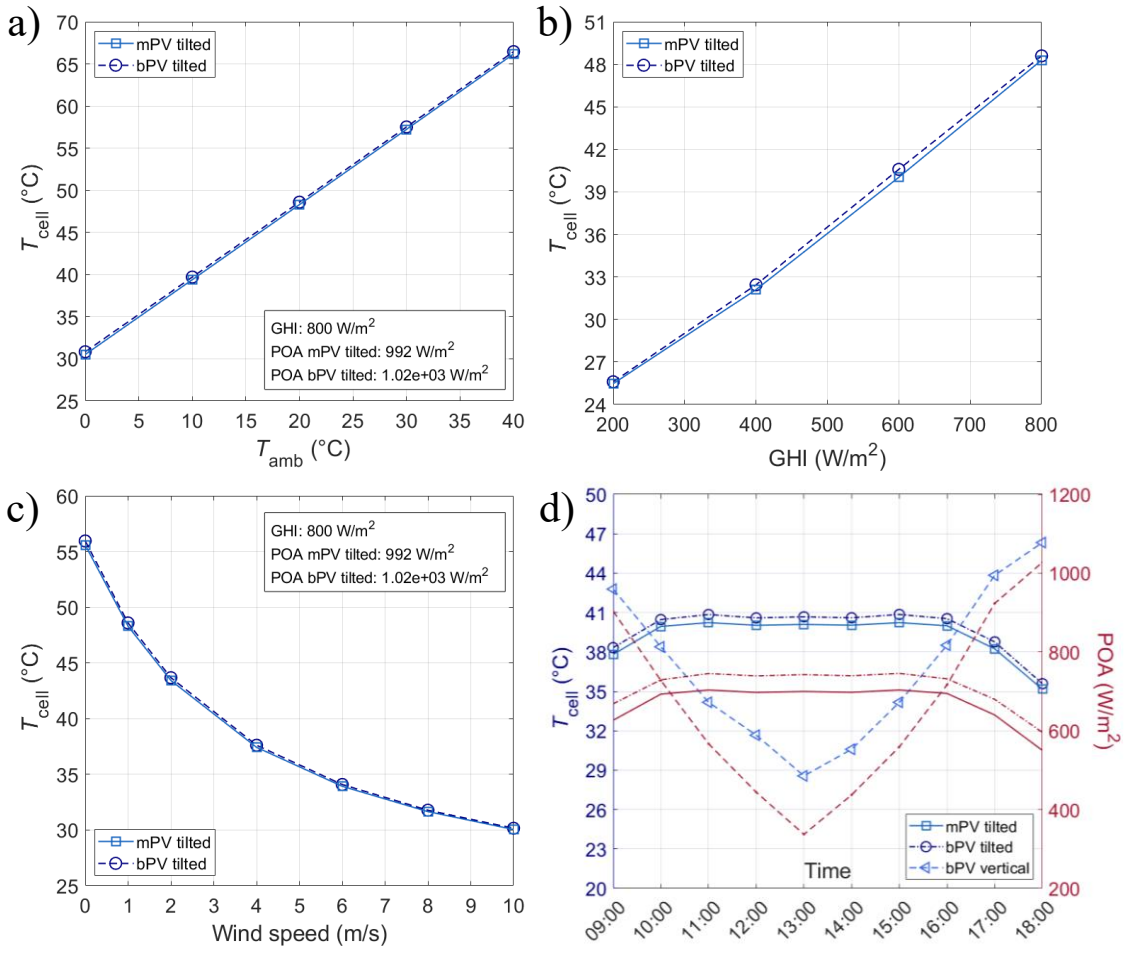

Figure 9: The effect of a) ambient temperature, b) irradiance, and c) wind speed on the average cell temperature of tilted monofacial (MPV) and bifacial (BPV) panel, and d) the steady-state temperature and POA irradiance of MPV, tilted BPV, and vertical BPV during the day. The POA irradiance was calculated from GHI assuming that the solar position corresponds to its typical position during a summer day (15th of June) in Helsinki (60.20° N, 24.96° E).

The effects of varying ambient conditions were similar for the MPV and tilted BPV panels (Figure 9). The average cell temperature of both panels increased as the ambient temperature increased (Figure 9a). The increase in the panel operating temperature was identical because the rate of change was 0.89°C/°C for both. Similarly, higher GHI led to higher average cell temperatures (Figure 9b). The operating temperature of both panels increased with a rate of change of 0.038°C/Wm^2. In contrast, the average temperature of MPV and tilted BPV cells decreased as the wind speed increased (Figure 9c). The increasing wind speed contributed to the cooling of the panel by increasing the convective heat transfer, resulting in lower operating temperatures. Under similar convective heat transfer conditions and GHI values, the absolute operating temperature of bifacial panel was presumed to be higher. Higher temperatures of BPV panels were expected because they are able to absorb irradiance also from their rear surface. Furthermore, the irradiance received by the panel is claimed to be one of the most important

factors affecting the temperature [43]. Based on the results shown in Figure 9, this assumption held true. However, the operating temperature of tilted BPV panel was not significantly higher than that of the MPV panel due to the relatively low installation angle of tilted BPV panel (Figure 5) which somewhat limits the absorption from the rear surface. Especially at noon, during which the operating temperatures were compared, the absorption from front surface dominates in the total absorption of tilted BPV panel. The operating temperature of tilted BPV was maximum 0.6°C higher than that of MPV panel under simulated environmental conditions. The differences in the panel operating temperatures are mainly due to differences in the irradiance received by the panel. In other words, the higher operating temperatures of bifacial panel arise from the higher POA irradiance and not from the characteristics of the panels, such as temperature and absorption coefficients, which were determined to be equal for all studied panels.

Figure 9d shows that the vertical BPV panel reached its highest steady-state temperature at different time of day than the MPV and tilted BPV panel. However, the average cell temperature of vertical BPV panel was lower than that of MPV or tilted BPV panel most of the day. At the points where the POA irradiance curves intersect, i.e., at the points where the environmental conditions and irradiance received by the panels are similar, the average cell temperature of the MPV panel was the highest and the average cell temperature of the vertical BPV panel was the lowest (Figure 9d).

5.2 Comparison of temperature model parameters for mono- and bifacial panels

The first objective of this thesis was to study the applicability of common PV temperature model parameters to bifacial solar panels. The model parameters of Sandia, Faiman, Mattei and TRNSYS models were determined by fitting these temperature models to the simulated average cell temperatures of mono- and bifacial panels. In the case of bifacial panels, the model parameters were determined for both tilted and vertical panels. The tilted panels are open-rack mounted and they have tilt angle of 30 degrees. Therefore, the convection conditions of MPV and tilted BPV are similar. The average cell temperatures were simulated in varying wind speed and POA irradiance values (Figure 10). The ambient temperature was 20°C in all cases. The input values for irradiance were calculated from GHI of 200−1000 W/m^2 at several angles of incidence.

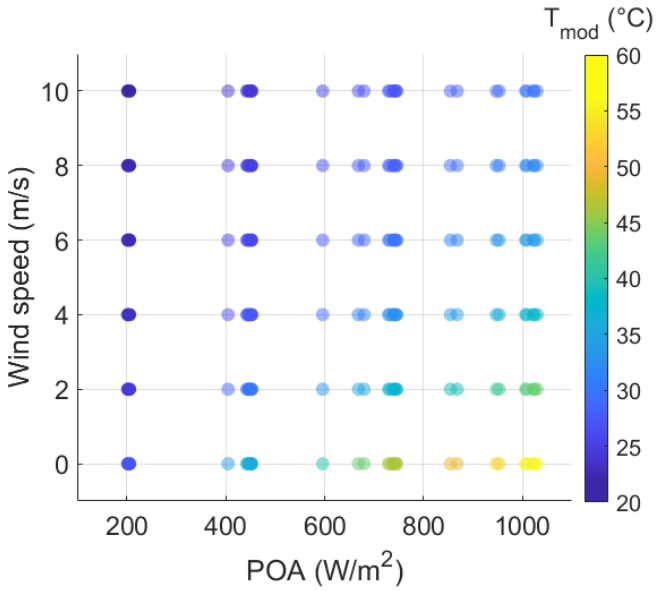

Figure 10: The environmental conditions at which the panel operating temperature was simulated. The color of the point represents the operating temperature of the panel.

Following the modeling of the panel operating temperatures, all temperature models were applied to that modeled data (Figure 11−Figure 14). For Sandia model, the data was fitted for the wind speeds between 0−4 m/s, 4−10 m/s, 0−10 m/s, as Figure 11 presents. For Faiman, Mattei and TRNSYS models, the data was only fitted for the wind speeds between 0−10 m/s (Figure 12−Figure 14). The model parameters can be determined from the slope and intercept coefficients of the fitted lines. The model parameters for all temperature models are presented in Table 8.

Table 8: Model parameters for the monofacial, and tilted and vertical bifacial panels determined by fitting temperature models to the simulated average cell temperature

Model	Model parameter	Monofacial	Tilted bifacial	Vertical bifacial
Sandia	***a***	-3.44	-3.48	-3.56
	b	-0.1265	-0.1264	-0.1385
Faiman	U_{L0} **[W/m²K]**	27.8	29.1	30.7
	U_{L1} **[Ws/m³K]**	7.28	7.59	9.46
Mattei	U_{PV} **[W/m²K]**	21.8	22.5	24.9
TRNSYS	U_{Loss} **[W/m²K]**	21.6	22.2	24.7

The values of the Sandia model parameters a and b determined for MPV and both BPV panels were within a similar magnitude (Table 8). In particular, the difference between the parameters of MPV and tilted BPV panels was minimal, as they differed only by less than 1 percent. The parameter b was expected to be almost equal for MPV and tilted BPV panels due to their similar convective heat transfer conditions. In contrast, the convective heat transfer coefficient of the rear surface of vertical BPV panel was determined to be twice as high that of tilted panels which explains the slightly different parameter b of vertical BPV panel. In addition, a smaller absolute value of a predicts higher panel operating temperatures. Because the absolute value of parameter a was smallest for the MPV panel, it was concluded that at close to zero wind speeds the MPV panel operates at the highest temperatures.

The predicted Sandia model parameters for MPV are quite consistent with those reported in literature [49], [79]. In the study by King et al. [49], in which Sandia temperature model was introduced, the empirically determined model parameters for different panel designs and mounting structures were reported. For an open rack mounted panel with a glass/cell/glass structure, the parameter a and b were -3.47 and -0.0594, respectively [49]. In this thesis, the parameters a and b for MPV panel were -3.44 and -0.127, respectively (Table 8). The predicted parameter a is almost equal to that reported by King et al. [49], and thus, when the effect of wind speed is minimal, i.e., at low wind speeds, the module temperature prediction is very similar using either literature value or the one predicted in this thesis. Since the b illustrates the decrease rate of the panel temperature as the wind speed increases, the difference in parameter b, is most likely due to the definition of the convective heat transfer coefficient in the model. Furthermore, the Koehl et al. [51] empirically determined model Sandia model parameters for crystalline silicon solar panels. They reported that the parameter a was -3.55 or -3.38−-3.37 and b was -0.13 or -0.12 depending on the geographical location of the PV system. These experimental parameters for monofacial silicon panels show an excellent agreement with the ones predicted in this thesis.

In addition to the models that are designed to study monofacial panels, Sandia National Laboratories have later developed models for estimating the performance of bifacial panels too [13]. The study implemented by Riley et al. [13] concluded that the temperature of bifacial panels can be sufficiently predicted using parameters initially determined for monofacial panels. The study was done for bifacial panels with a tilt angle between 15 and 45 degrees. The results of this thesis support this finding. Especially in the case of tilted BPV panels, the Sandia model parameters determined in this thesis were very similar to those of MPV panels.

Moreover, Mannino et al. [14] applied Sandia model to BPV panels. In this study, the tilt angle of the BPV panels was 37.5° [14]. They showed that, when the parameters reported by King et al. [49] (a=-3.47 and b=-0.0594) were used for BPV panel temperature estimation, the accuracy of estimation was lower than with the optimized parameters [14]. A similar study that utilized the data by Mannino et al. [14] reported that the optimal parameter a for BPV panels was around -3.79 and b was -0.0699 [80].

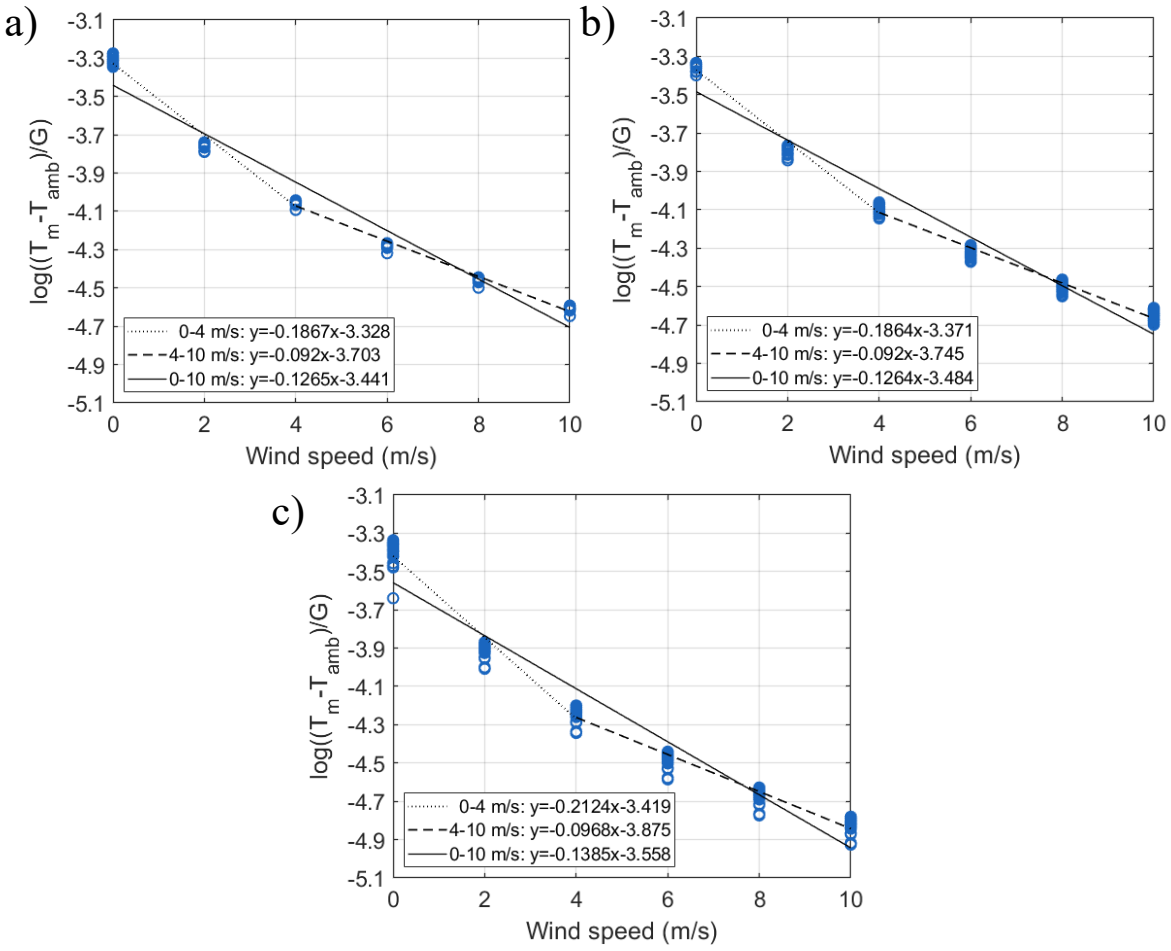

Figure 11: Sandia model fitted to the simulated average cell temperature of a) monofacial, b) tilted bifacial, c) vertical bifacial panels.

Comparison of Faiman model parameters showed that the parameter U_{L0} was around 5 higher for tilted BPV than for MPV (Table 8). Correspondingly, the parameter U_{L1} was around 4 percent higher for tilted BPV. The parameter U_{L0} of vertical BPV panel was within the same order of magnitude as those of MPV and tilted BPV panels. Thus, at low wind speeds, the predicted temperature of all panels would be similar. However, the U_{L1} was around 30 percent higher for vertical BPV panel than for MPV panel. As mentioned, U_{L1} determines the effect of wind speed on the panel temperature. The difference in the parameter U_{L1} between tilted and

vertical panels arise from the magnitude of convective heat transfer coefficient on the rear surface.

The experimentally determined Faiman model parameters for MPV silicon solar panels reported in the literature [50], [79] show a good agreement with the ones predicted in this thesis (U_{L0}=27.8 W/m^{2}K, U_{L1}=7.28 Ws/m^{3}K, Table 8). The study by Faiman [50] concluded that average value of U_{L0} was 24.9 ± 1.0 W/m^{2}K and U_{L1} was 7.00 ± 0.55 Ws/m^{3}K for mono- and polycrystalline silicon solar panels. Furthermore, Koehl et al. [51] reported that U_{L0} was close to 27 W/m^{2}K or 28 W/m^{2}K and U_{L1} was 6.11− 6.24 or 7.77 Ws/m^{3}K depending on the geographical location of the measured PV system.

In the literature, some Faiman model parameters for the BPV silicon panels have also been reported. For instance, Mannino et al. [14] applied Faiman model to the experimental data from tilted BPV panels, similarly as they applied Sandia model. They stated that accuracy of temperature estimation increased when model parameters, that were optimized using the data from BPV panels, were utilized [14]. Additionally, Grisanti et al. [80] showed that the optimal U_{L0} was notably higher and U_{L1} notably lower for BPV panel than for MPV panel. Higher value of U_{L0} indicates that at low wind speeds the BPV panel could to operate at lower temperatures than that of MPV panel. Lower value of U_{L1}, on the other hand, indicates that the wind speed affects the cooling of BPV panel less. As in the study of Grisanti et al. [80], the parameter U_{L0} predicted in this study was higher for both BPV panels than for MPV panel. In contrast, in this thesis the effect of wind speed (parameter U_{L1}) on the temperature of tilted BPV and MPV panels was very similar, because of the identical convective heat transfer coefficients.

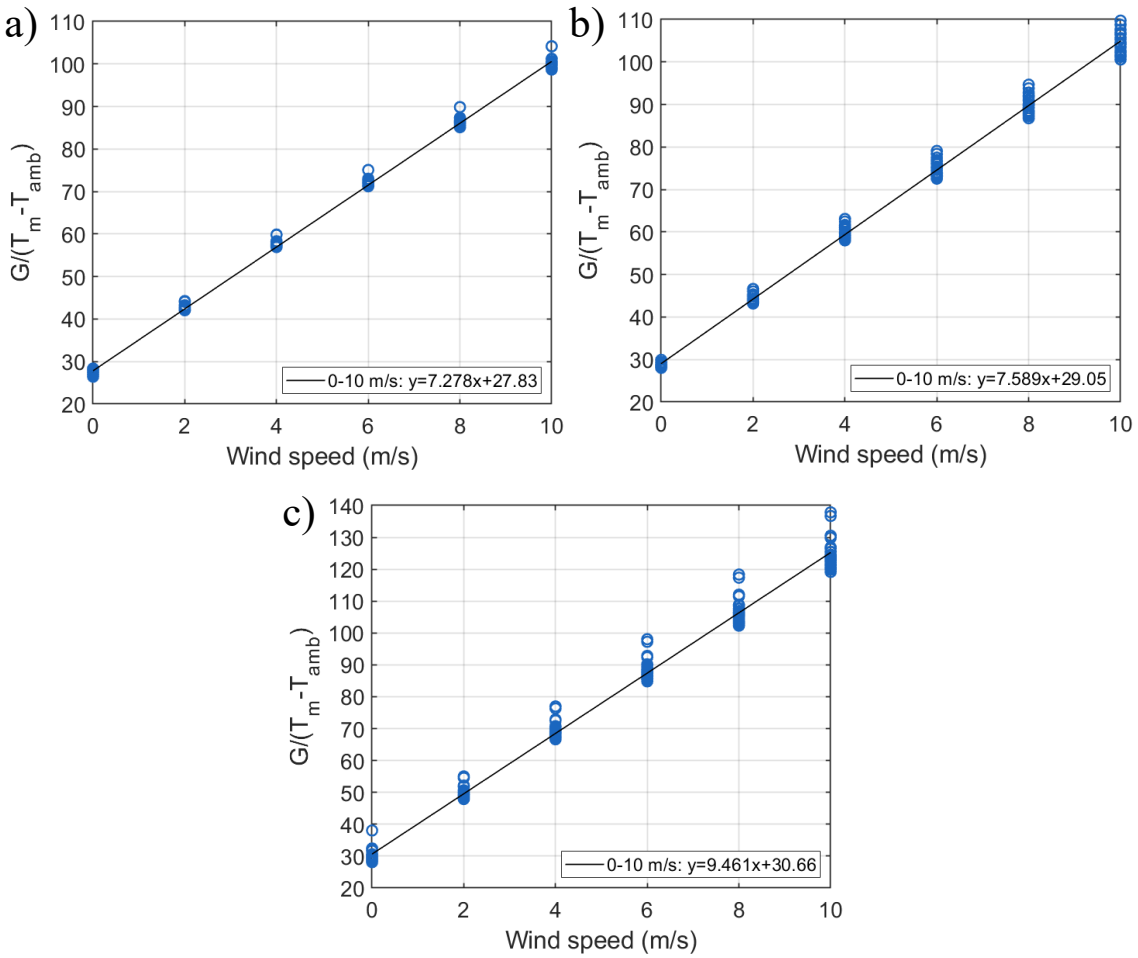

Figure 12: Faiman model fitted to the simulated average cell temperature of a) monofacial, b) tilted bifacial, c) vertical bifacial panels.

The parameters for Mattei and TRNSYS models illustrate the heat losses due to convective heat transfer. The other characteristics of the panel are taken into account in the parameters β, α_{tot} and $\mathrm{PCE}_{\mathrm{ref}}$. When the wind speed was set to 1 m/s, Mattei parameter U_{PV} was 3 % and 14 % higher for the tilted BPV and vertical BPV panels than for the MPV panel, respectively (Table 8). The results were almost identical in the case of TRNSYS parameter U_{Loss} (Table 8). The slight difference in both Mattei and TRNSYS parameters of tilted MPV and BPV panels mainly arise from $\mathrm{PCE}_{\mathrm{ref}}$, because the β, α_{tot} and h were determined similarly for both. Furthermore, the difference in the parameters of tilted and vertical panels arise from the h of the panel rear surface.

The study by Mattei et al. [51] showed two alternative values to the Mattei model parameter U_{PV}. They stated that at a wind speed of 1 m/s U_{PV} is either 27 or 28.9 W/m^{2}K depending on the value of α_{tot}. Furthermore, these parameters depend on wind speed as follows: $U_{\mathrm{PV}} = 2.9v + 24.1$ or $U_{\mathrm{PV}} = 2.3v + 26.6$ [51]. The parameter U_{PV} predicted for MPV panel in this

thesis is notably smaller than either of parameters reported by Mattei et al. [51]. However, the heat losses were defined differently in Mattei model and the physical device thermal model presented in this thesis. As mentioned, Mattei model explicitly ignores radiative heat transfer. The physical device thermal model, on the other hand, includes the radiative heat transfer. Thus, the heat loss parameter of Mattei model and convective heat transfer coefficient of physics-based thermal model are not directly comparable.

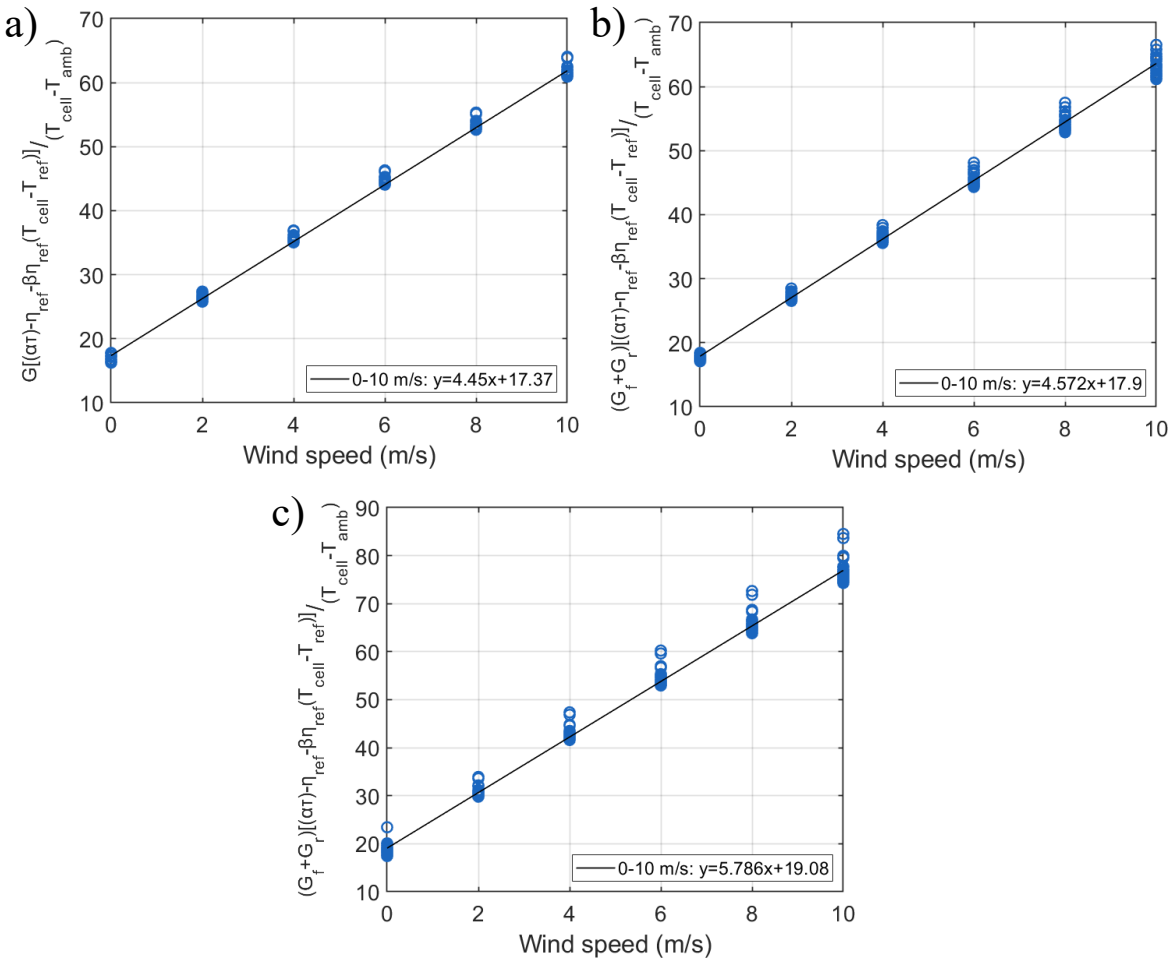

Figure 13: Mattei model fitted to the simulated average cell temperature of a) monofacial, b) tilted bifacial, c) vertical bifacial panels.

In the literature TRNSYS model is often applied to NOCT (nominal operating cell temperature) conditions [53], [81], [82], that is the ambient temperature of 20 °C, wind speed of 1 m/s, and total irradiance of 800 W/m^2 [83]. At NOCT conditions $U_{\mathrm{Loss}} = \alpha_{\mathrm{tot}} G_{\mathrm{NOCT}} / (T_{\mathrm{m,NOCT}} - T_{\mathrm{amb,NOCT}})$ [53]. Based on the previous equation the U_{Loss} would be approximately 27 W/m^{2}K for polycrystalline silicon panel with NOCT temperature of 47°C. For NOCT values between 44°C and 49°C, the U_{Loss} would range around 25–30 W/m^{2}K. It was stated that model with NOCT based U_{Loss} provides a reasonable accuracy for temperature estimation of free-standing

panels [53]. However, NOCT based U_{Loss} is a rough approximation, and thus, it should not be applied for temperature estimations of different type of mounting configurations, especially if the convective cooling on the rear surface is limited [53]. The model with NOCT based U_{Loss} overestimates the operating temperature notably, if the environmental conditions on both sides of the panel are not similar [53]. In this thesis the effect of wind speed at the rear surface of the panel was determined to be lower for tilted MPV and BPV panels, and therefore, NOCT based U_{Loss} is not comparable with U_{Loss} predicted for tilted panels in this thesis.

Furthermore, Khan et al. [11] reported U_{Loss} for bifacial solar panels. The value of parameter U_{Loss} was 21.5 $\mathrm{m^2K}$ for silicon heterojunction BPV panel [11]. The tilt angle of the panel was not specified. The results of this thesis show an excellent agreement with the literature values. The U_{Loss} predicted for tilted BPV panel in this thesis differs from that reported in literature by only around 3 percent.

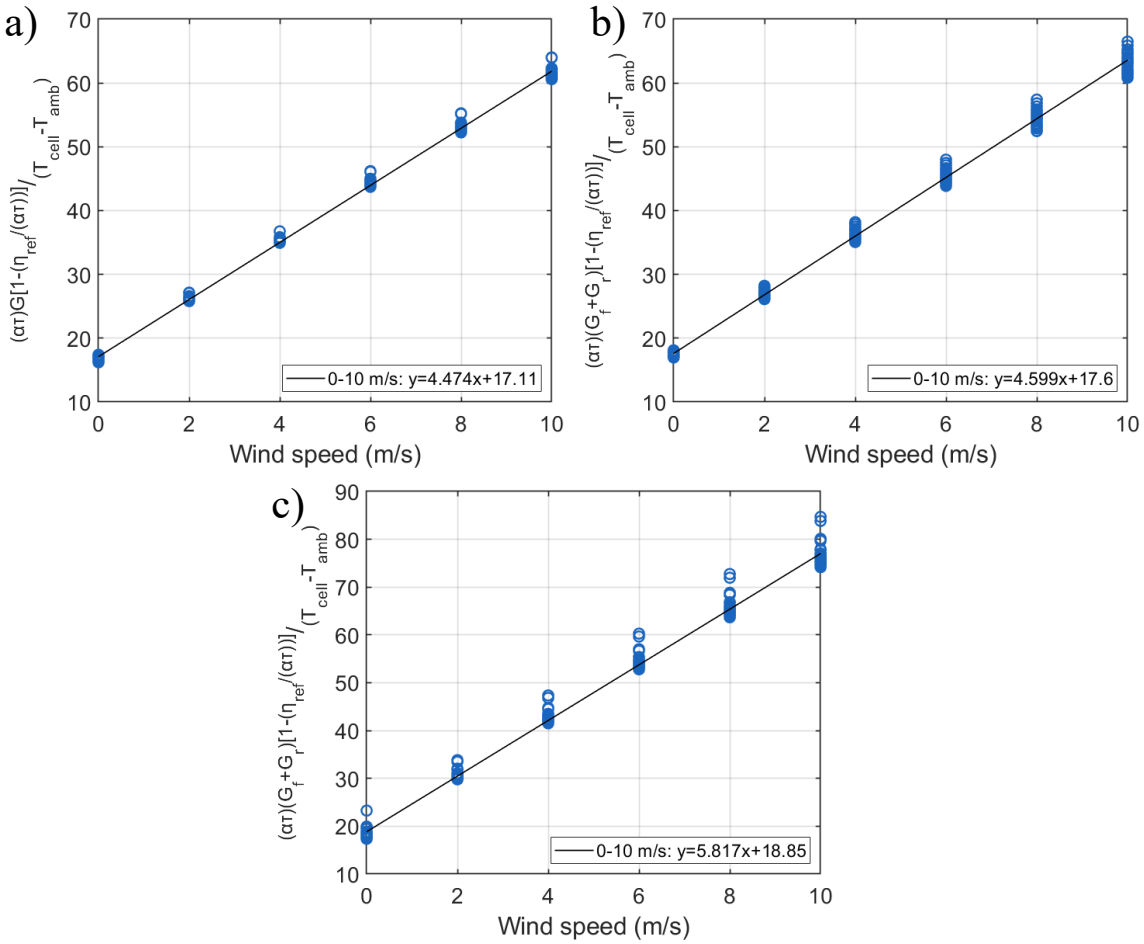

Figure 14: TRNSYS model fitted to the simulated average cell temperature of a) monofacial, b) tilted bifacial, c) vertical bifacial panels.

5.3 Evaluation of the use of GHI and calculated POA irradiance in photovoltaic module temperature models

The second objective of this thesis was to study the use of GHI and the calculated POA irradiance in the temperature estimations instead of the commonly utilized measured POA irradiance. The calculated POA was determined from GHI using irradiance model described in Section 4.4. The suitability of GHI and the calculated POA irradiance for predicting the panel operating temperature was investigated from two perspectives. To begin with, the accuracy of panel temperature estimation, when GHI and the calculated POA irradiance were applied to the common temperature models, was determined. Following that, the accuracy of those temperature estimations was compared to the temperature estimation utilizing the measured POA irradiance. Moreover, it was examined whether GHI can be used to determine the temperature model parameters sufficiently.

5.3.1 Accuracy of operating temperature estimation using GHI and calculated POA irradiance

The accuracy of Sandia (Eq. 11), Faiman (Eq. 15), Mattei (Eq. 17), and TRNSYS (Eq. 19) temperature model estimations was evaluated for different irradiance input values. The evaluation was done by comparing the predicted panel temperatures with those measured from bi- and monofacial panels at TUAS' and FMI's sites as Figure 15 and Figure 16 present. The measured ambient temperatures, wind speeds, and both GHI and POA irradiances were applied to temperature models. Model parameters, determined in the literature for monofacial panels, were used in Sandia, Faiman and Mattei models [49], [50], [51]. TRNSYS model utilized U_{Loss} value of 21.5 W/m^{2}K that is also reported to be used for estimating the operating temperatures of bifacial panels [11]. The power conversion efficiency required in Mattei and TRNSYS models, and the temperature coefficient required in Mattei model were selected to match the values reported by the manufacturer of the reference panels at TUAS' and FMI's sites (Table 5). The temperature estimation accuracies were reported for BPV panel (Table 9) and MPV panel (Table 10), when GHI, and both calculated and measured POA irradiance were used in the temperature models.

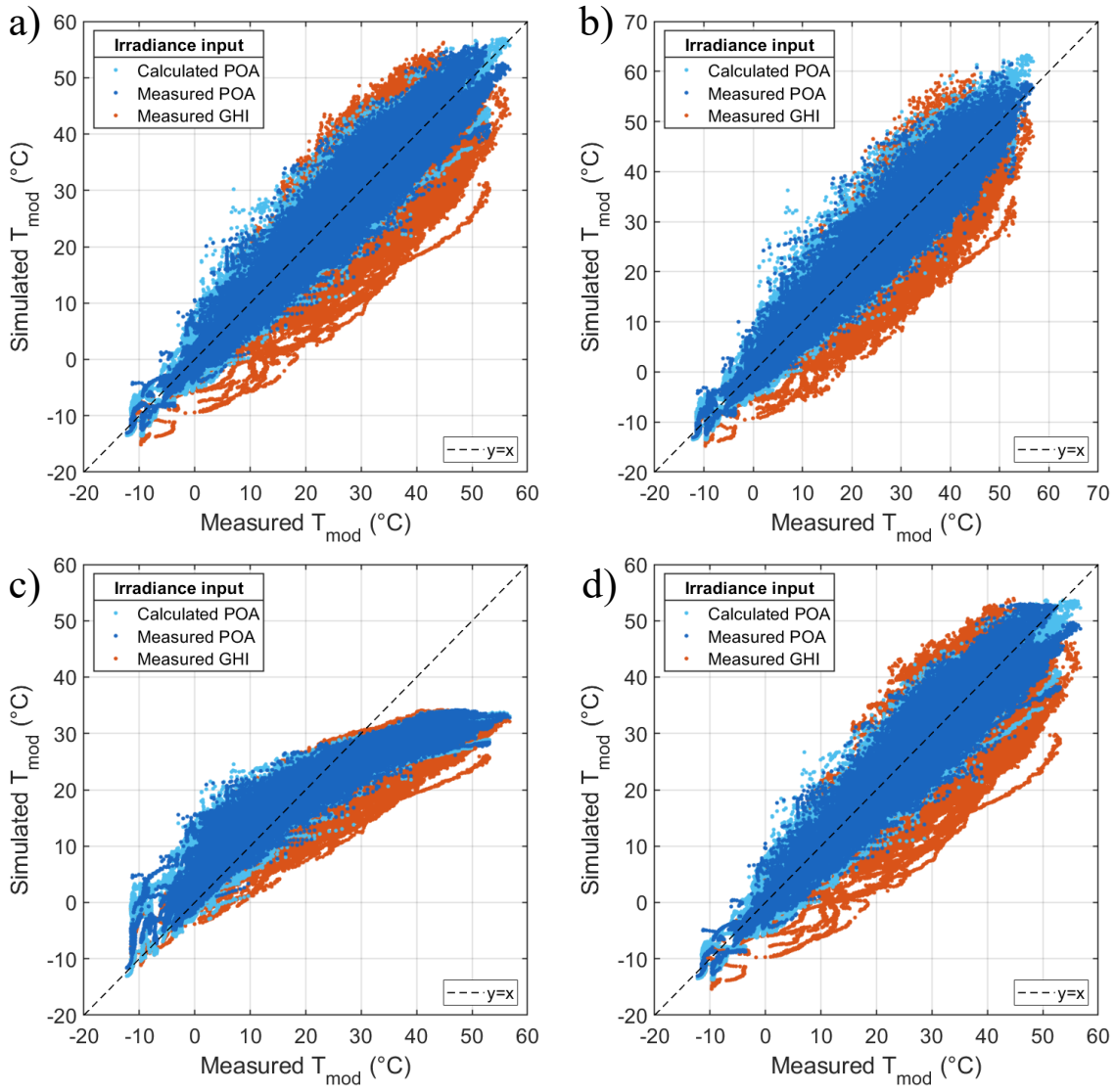

Figure 15: The module temperature evaluated using a) Sandia, b) Faiman, c) Mattei and d) TRNSYS models as a function of the module temperature measured from vertical bifacial panel at TUAS' measurement site.

Table 9: Evaluation metrics for the temperature models predicting the temperature of bifacial panel when GHI, and the calculated and measured POA irradiances were used as a model input for irradiance.

Temperature model	Model input	MAE [°C]	RMSE [°C]	Corr. Coeff.	Bias [°C]
Sandia	Meas. POA	2.1	2.8	0.979	0.28
	Calc. POA	2.1	2.9	0.981	-0.45
	Meas. GHI	3.9	5.8	0.915	1.8
Faiman	Meas. POA	2.1	2.9	0.979	0.35
	Calc. POA	2.2	3.1	0.978	-0.39
	Meas. GHI	3.8	5.6	0.923	2.0
Mattei	Meas. POA	3.7	5.6	0.958	2.0
	Calc. POA	3.9	5.7	0.945	1.6
	Meas. GHI	4.3	6.6	0.927	2.8
TRNSYS	Meas. POA	2.2	3.0	0.976	0.68
	Calc. POA	2.1	2.9	0.978	-0.0094
	Meas. GHI	4.0	6.0	0.910	2.1

The results showed that the temperature of bifacial panels can be predicted with good accuracy using most of the temperature models (Table 9). However, the temperature estimation of Mattei model was quite inaccurate. Both the MAE and RMSE were significantly higher for Mattei model estimation than for other models, when the calculated and measured POA irradiances were used in the temperature prediction. Furthermore, the lower correlation coefficient in comparison with the other models revealed that the temperatures estimated using Mattei model show the worst correlation with the ideal relationship between predicted and measured values (Table 9). Figure 15c illustrates that Mattei model does not fit to the data particularly well. Mattei model seemed to underestimate the BPV panel temperature, especially at higher panel temperatures (Figure 15c). Correspondingly, it underestimated the temperature of MPV panel (Figure 16c). Similar findings are reported in the literature because Mattei model is claimed to underestimate the operating temperature of panel at high irradiances [84].

Moreover, the comparison of predicted and measured values showed that the panel temperature can also be moderately estimated when GHI is applied to the model (Table 9). The MAE of temperature estimations was between 3.8°C and 4.3°C for all the models while RMSE varied

between 5.6°C and 6.6°C when GHI was used. However, the accuracy of temperature estimation was notably higher when the measured POA was applied to the model. For Sandia, Faiman, and TRNSYS model, the MAE of temperature estimations increased by 1.7–1.8°C when using GHI instead of the measured POA irradiance. Correspondingly, RMSE increased by 2.7–3.0°C. For Mattei model, the difference between temperature estimation accuracy, when using GHI and the measured POA irradiance, was notably lower because MAE and RMSE increased only by 0.6°C and 1.0°C, respectively. Furthermore, the calculated POA irradiance seemed to be well suited for estimating module temperatures. The MAE and RMSE of temperature estimation were both less than 0.2°C higher when the calculated POA irradiance was applied to Sandia, Faiman and Mattei models instead of the measured POA irradiance. In TRNSYS model, the use of calculated POA irradiance resulted in even better accuracy than the use of measured POA irradiance.

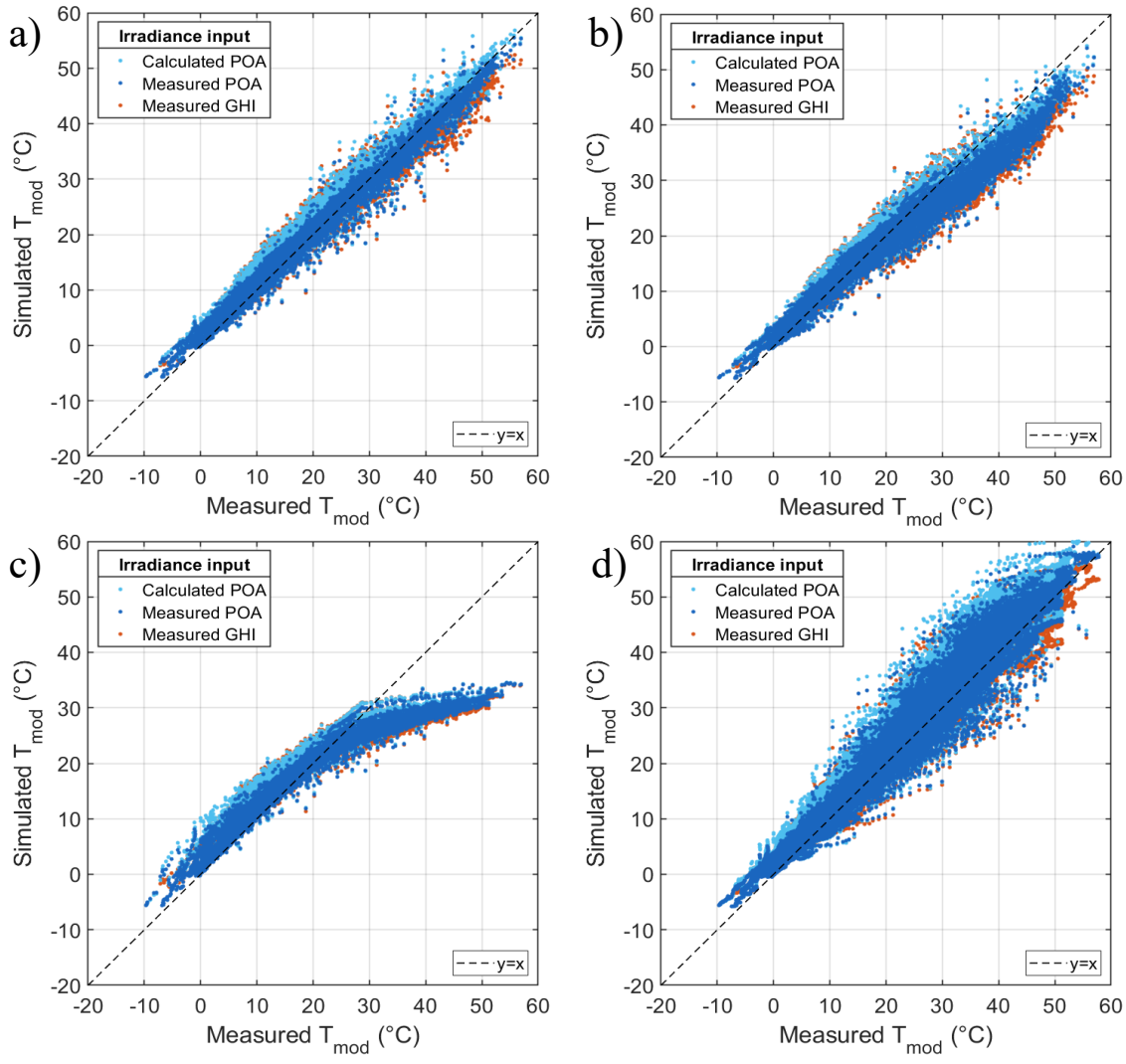

Figure 16: The module temperature evaluated using a) Sandia, b) Faiman, c) Mattei and d) TRNSYS models as a function of the module temperature measured from vertical bifacial panel at TUAS' measurement site.

Table 10: Evaluation metrics for the temperature models predicting the temperature of monofacial panel when GHI, and the calculated and measured POA irradiances were used as a model input for irradiance.

Temperature model	Model input	MAE [°C]	RMSE [°C]	Corr. Coeff.	Bias [°C]
Sandia	Meas. POA	1.3	1.7	0.992	-0.26
	Calc. POA	1.8	2.3	0.987	-1.3
	Meas. GHI	1.9	2.5	0.981	-0.48
Faiman	Meas. POA	2.1	3.0	0.985	1.0
	Calc. POA	1.9	2.6	0.982	0.24
	Meas. GHI	2.4	3.5	0.972	0.87
Mattei	Meas. POA	3.3	5.3	0.955	1.2
	Calc. POA	3.6	5.3	0.942	0.66
	Meas. GHI	3.6	5.5	0.939	0.96
TRNSYS	Meas. POA	1.9	2.5	0.988	-1.5
	Calc. POA	3.0	4.0	0.980	-2.8
	Meas. GHI	2.3	3.1	0.978	-1.8

In the case of monofacial panels, the temperatures predicted with the Sandia, Faiman, TRNSYS models showed a good agreement with the ones measured from FMI's panels (Figure 16). This was expected because the temperature models and their parameters are initially designed for MPV panels. Moreover, the decrease in the accuracy of MPV panel (Table 10) temperature estimation was lower in comparison with that of BPV panel (Table 9) when GHI was applied to the model instead of the measured POA irradiance. For instance, the MAE of MPV panel temperature estimation increased only 0.3–0.6°C when GHI was applied to Sandia, Faiman and TRNSYS models instead of the measured POA irradiance. Correspondingly for BPV panel, MAE increased 1.7–1.8°C when GHI was applied to those three models. The decrease in the temperature estimation accuracy of Mattei model was lower than with the other models in terms of both MAE and RMSE. Additionally, the temperature estimation accuracy of MPV panel was almost as high using the calculated POA as using the measured one which was also the case with BPV panels. The MAE and RMSE of Sandia, Faiman and Mattei model estimations, using the measured and calculated POA, differed less than 0.5°C and 0.6°C. In the case of TRNSYS model, the difference between estimation accuracies was higher.

5.3.2 Accuracy of temperature model parameter prediction using GHI

Moreover, the use of GHI for determining the common temperature model parameters was investigated. To do that, the average cell temperature of tilted and vertical BPV panels was applied to the temperature models similarly as in Section 5.2. The model fitting was done by applying both GHI and the calculated POA irradiance to the model. The absolute difference between parameters, that were predicted using GHI and the calculated POA irradiance, was studied with the respect of AOI (Figure 17 and Figure 18).

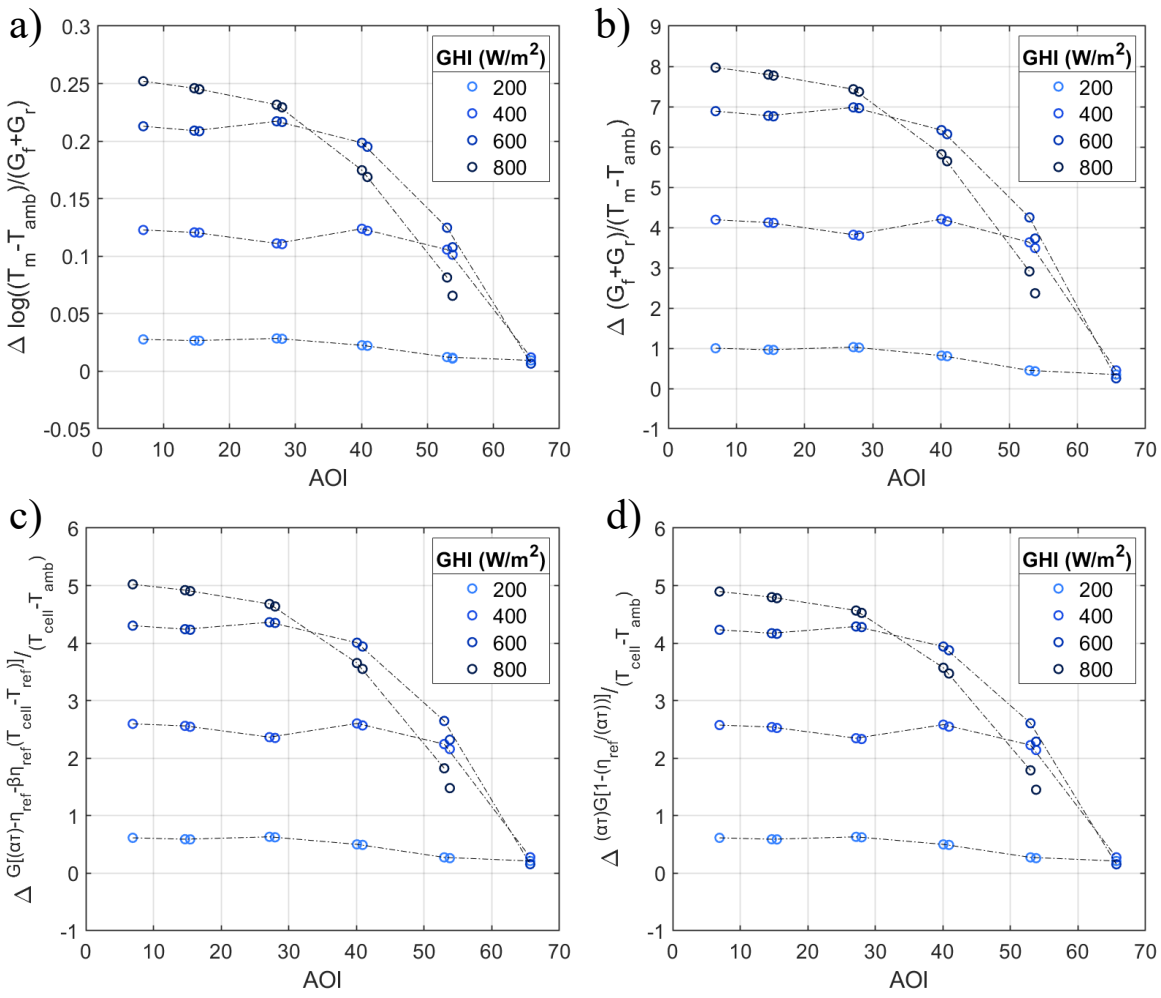

Figure 17: The absolute difference between parameters predicted using calculated POA irradiance and GHI, presented as a function of the angle of incidence (AOI). The parameters were predicted for a) Sandia, b) Faiman, c) Mattei, and d) TRNSYS models utilizing the simulated data of tilted bifacial panel. Different colors of the points illustrate different GHI values.

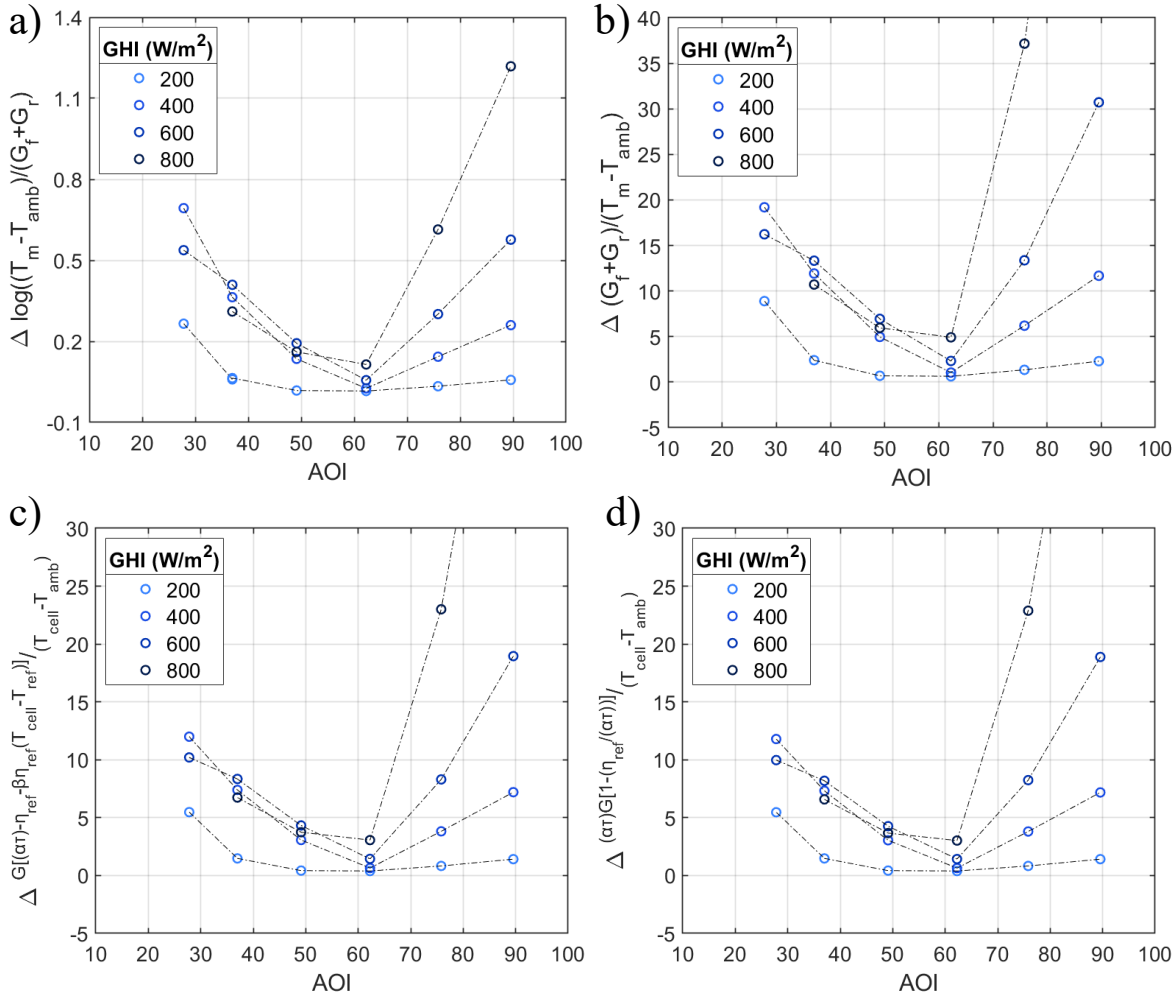

Figure 18: The absolute difference between parameters predicted using calculated POA irradiance and GHI, presented as a function of the angle of incidence (AOI). The parameters were predicted for a) Sandia, b) Faiman, c) Mattei, and d) TRNSYS models utilizing the simulated data of vertical bifacial panel. Different colors of the points illustrate different GHI values. When GHI is 800 W/m^2 and AOI is around 90 degrees, the point representing the difference between parameters is not shown in the figure (b, c, d).

The results showed, the model parameters cannot be predicted for any common temperature model with a reasonable accuracy using GHI because they strongly depend on the AOI. Especially in the case of vertical BPV panel, the variation in the model parameters between different AOIs was significant (Figure 18). However, for both tilted and vertical BPV, the parameters determined using GHI were closer to the parameters determined using the calculated POA irradiance, when the AOI was higher (Figure 17 and Figure 18). Furthermore, the difference between POA- and GHI-based parameters was smaller at lower GHI for most AOIs. Especially, the temperature of tilted BPV panel could be estimated with good accuracy using GHI when the GHI levels were close to 200 W/m^2 (Figure 17). In the case of tilted BPV, the parameters predicted using GHI and the calculated POA irradiance were closest to each other when the AOI was around 66 degrees (Figure 17). Correspondingly, in the case of vertical BPV,

the parameters were closest to each other when the AOI was around 63 degrees (Figure 18). Thus, the GHI-based model parameters of both tilted and vertical BPV could be most accurately predicted when AOI was close to 65 degrees. Additionally, a relatively good prediction could be achieved when AOI was around 50–55 degrees.

6 Research limitations

The present thermal model was successfully used to study the temperatures of MPV and BPV panels with different installation configurations and ambient conditions. The simulated data was utilized to evaluate the suitability of different parameters for temperature modeling of solar panels. However, the study had some limitations which will be briefly discussed here.

In this thesis, the physical properties of MPV and BPV cells were defined similarly in the thermal model, apart from the power conversion efficiency of the rear surface of BPV, to enable easy comparison. However, bifacial solar cell technologies have often been reported to have lower temperature coefficients and higher efficiencies than monofacial ones (Table 1). A lower temperature coefficient indicates a lesser decrease in the cell efficiency as the temperature increases, and thus, it results in lower operating temperatures as Figure 19 demonstrates. This is a noteworthy detail to consider in the future research.

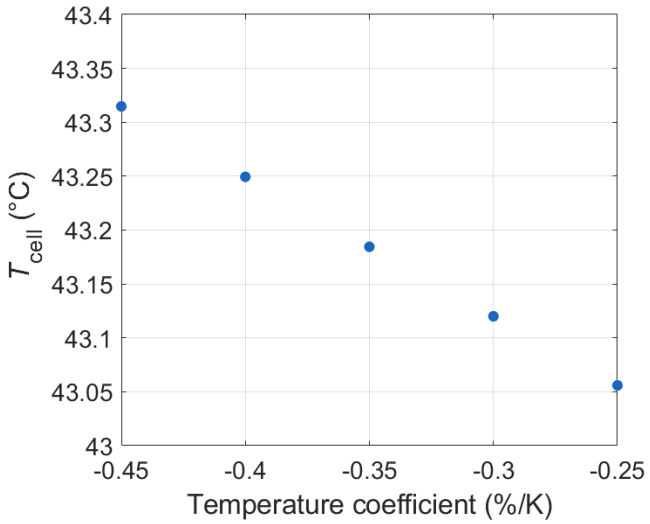

Figure 19: The average cell temperature as a function of the temperature coefficient of efficiency at $T_{amb} = 20$ °C, $G_{POA} = 800$ W/m^2, and $v = 1$ m/s.

Furthermore, as discussed in Section 4.5.3, the present thermal model does not account the wind direction. The effect of wind direction could be included in the thermal model to enable more accurate modeling of the convective cooling at different surfaces of the panel. This could especially improve the accuracy of thermal model of the vertically installed solar panels. Refining the thermal model, for instance in terms of wind direction, would enable to determine more accurate temperature model parameters based on that simulated data. More accurate temperature parameters would, in turn, improve accuracy of the power predictions in future studies.

7 Conclusions

This thesis focused on evaluating the applicability of existing PV module temperature models and their parameters to estimate the operating temperatures of bifacial solar panels. The model parameters of Sandia, Faiman, Mattei, and TRNSYS models were successfully predicted for the mono- and bifacial panels using the temperature data simulated with the present physical device thermal model. It was found that the parameters of mono- and bifacial panels with identical installations differ maximum 5 % for all studied temperature models. However, the modeled parameters of vertical bifacial panels were found to be 10–30 % higher than those of monofacial tilted panels. Thus, the model parameters, initially determined for the monofacial panels, seemed to be suitable for predicting the temperatures of the conventionally mounted bifacial panels but not those of vertically mounted. Therefore, the model parameters determined, in particular for vertical installations, should be further evaluated.

Furthermore, this thesis aimed to compare the accuracy of temperature estimations when GHI and the calculated POA irradiance were applied to the existing temperature models instead of the measured POA irradiance. Based on the obtained results, the use of GHI in any of the studied temperature models cannot be primarily recommended, because that consistently led to the worst accuracy in terms of MAE and RMSE. However, the accuracy of temperature estimation of MPV panel did not decrease as significantly as that of BPV panel when GHI was used instead of the measured POA irradiance. The MAE increased less than 0.6°C for monofacial panels but 1.7–1.8°C for bifacial panels. Thus, if POA irradiance data is lacking, the use of GHI in the temperature estimations of monofacial PV panels can be considered.

On the contrary, it is advisable to use the calculated POA irradiance in the temperature models. The accuracy loss was minimal when using the calculated POA instead of the measured one. For instance, the MAE and RMSE of BPV panel temperature estimations differed only less than 0.2°C. Similarly, MAE and RMSE of MPV panel temperature estimations differed less than 0.6°C, regardless of whether the calculated or measured POA irradiance was applied to the studied temperature models (except TRNSYS). The measured POA irradiance depends on system specifications and, thus, it must be measured for each system separately. Therefore, the use of calculated POA irradiance in temperature estimation can save resources without significantly compromising the accuracy.

Moreover, GHI should not be used to determine the model parameters of the common temperature models. The parameters that were predicted using GHI depended strongly on the

AOI of sun rays, especially at high GHI values, unlike the parameters that were predicted using the calculated POA irradiance. Thus, the estimation of the panel operating temperatures would mostly be unreliable with the GHI-based model parameters.

The main contribution of this thesis was that it confirmed that: 1) the temperature model parameters initially determined for MPV panels are suitable for predicting the operating temperatures of conventionally mounted BPV panels, and 2) the use of calculated POA irradiance leads to almost as accurate module temperature estimations as the use of measured POA irradiance. Overall, this thesis provided information about suitability of different parameters for temperature modeling of solar panels and, thus, created a solid foundation to further research on the topic.

References

[1] IRENA, “Future of solar photovoltaic: Deployment, investment, technology, grid integration and socio-economic aspects,” International Renewable Energy Agency, 2019.

[2] IEA-PVPS, “Snapshot of Global PV Markets 2022,” 2022. Accessed: Dec. 09, 2024. [Online]. Available: https://iea-pvps.org/snapshot-reports/snapshot-2022/

[3] W. Gu, T. Ma, S. Ahmed, Y. Zhang, and J. Peng, “A comprehensive review and outlook of bifacial photovoltaic (bPV) technology,” *Energy Convers Manag*, vol. 223, Nov. 2020, doi: 10.1016/j.enconman.2020.113283.

[4] A. Garrod and A. Ghosh, “A review of bifacial solar photovoltaic applications,” Dec. 01, 2023, *Higher Education Press Limited Company*. doi: 10.1007/s11708-023-0903-7.

[5] “International Technology Roadmap for Photovoltaic (ITRPV) 2017 Results,” 2018. [Online]. Available: www.itrpv.net.

[6] “International Technology Roadmap for Photovoltaic (ITRPV) 2021 Results,” 2022.

[7] S. Jouttijärvi, G. Lobaccaro, A. Kamppinen, and K. Miettunen, “Benefits of bifacial solar cells combined with low voltage power grids at high latitudes,” Jun. 01, 2022, *Elsevier Ltd*. doi: 10.1016/j.rser.2022.112354.

[8] P. K. Sahu, J. N. Roy, and C. Chakraborty, “Performance assessment of a bifacial PV system using a new energy estimation model,” *Solar Energy*, vol. 262, Sep. 2023, doi: 10.1016/j.solener.2023.111818.

[9] M. T. Patel, R. A. Vijayan, R. Asadpour, M. Varadharajaperumal, M. R. Khan, and M. A. Alam, “Temperature-dependent energy gain of bifacial PV farms: A global perspective,” *Appl Energy*, vol. 276, Oct. 2020, doi: 10.1016/j.apenergy.2020.115405.

[10] W. Gu, T. Ma, M. Li, L. Shen, and Y. Zhang, “A coupled optical-electrical-thermal model of the bifacial photovoltaic module,” *Appl Energy*, vol. 258, Jan. 2020, doi: 10.1016/j.apenergy.2019.114075.

[11] M. R. Khan, M. T. Patel, R. Asadpour, H. Imran, N. Z. Butt, and M. A. Alam, “A review of next generation bifacial solar farms: Predictive modeling of energy yield, economics, and reliability,” Aug. 01, 2021, *IOP Publishing Ltd*. doi: 10.1088/1361-6463/abfce5.

[12] X. Sun, M. R. Khan, C. Deline, and M. A. Alam, “Optimization and performance of bifacial solar modules: A global perspective,” *Appl Energy*, vol. 212, pp. 1601–1610, Feb. 2018, doi: 10.1016/j.apenergy.2017.12.041.

[13] D. Riley *et al.*, “A Performance Model for Bifacial PV Modules,” in *IEEE 44th Photovoltaic Specialist Conference (PVSC)*, IEEE, Jun. 2017.

[14] G. Mannino, G. M. Tina, M. Cacciato, L. Todaro, F. Bizzarri, and A. Canino, “Experimental assessment of temperature estimation models of bifacial photovoltaic modules,” in *Conference*

Record of the IEEE Photovoltaic Specialists Conference, Institute of Electrical and Electronics Engineers Inc., 2022, pp. 214–216. doi: 10.1109/PVSC48317.2022.9938792.

[15] W. D. Callister Jr. and D. G. Rethwisch, *Callister's Materials Science and Engineering: An Introduction*, 10th edition. Wiley.

[16] IEA-PVPS, "Bifacial Photovoltaic Modules and Systems: Experience and Results from International Research and Pilot Applications," 2021. [Online]. Available: www.iea-pvps.org

[17] T. S. Liang *et al.*, "A review of crystalline silicon bifacial photovoltaic performance characterisation and simulation," *Energy Environ Sci*, vol. 12, no. 1, pp. 116–148, Jan. 2019, doi: 10.1039/c8ee02184h.

[18] L. Wang, Y. Tang, S. Zhang, F. Wang, and J. Wang, "Energy yield analysis of different bifacial PV (photovoltaic) technologies: TOPCon, HJT, PERC in Hainan," *Solar Energy*, vol. 238, pp. 258–263, May 2022, doi: 10.1016/j.solener.2022.03.038.

[19] T. M. Mahim, A. H. M. A. Rahim, and M. M. Rahman, "Review of Mono-and Bifacial Photovoltaic Technologies: A Comparative Study," *IEEE J Photovolt*, vol. 14, no. 3, pp. 375–396, May 2024, doi: 10.1109/JPHOTOV.2024.3366698.

[20] A. Hubner, A. G. Aberle, and R. Hezel, "TEMPERATURE BEHAVIOR OF MONOFACIAL AND BIFACIAL SILICON SOLAR CELLS."

[21] X. Cheng *et al.*, "Comparative Study on Temperature Coefficients of Al-BSF Solar Cells and PERC Solar Cells," in *2019 IEEE 46th Photovoltaic Specialists Conference (PVSC)*, IEEE, 2019.

[22] H. Wang, X. Cheng, and H. Yang, "Temperature Coefficients and Operating Temperature Verification for Passivated Emitter and Rear Cell Bifacial Silicon Solar Module," *IEEE J Photovolt*, vol. 10, no. 3, pp. 729–739, May 2020, doi: 10.1109/JPHOTOV.2020.2974289.

[23] N. Kumari, S. K. Singh, S. Kumar, and V. K. Jadoun, "Performance analysis of partially shaded high-efficiency mono PERC/mono crystalline PV module under indoor and environmental conditions," *Sci Rep*, vol. 14, no. 1, Dec. 2024, doi: 10.1038/s41598-024-72502-z.

[24] S. M. F. Zhang *et al.*, "Illumination-dependent temperature coefficients of the electrical parameters of modern silicon solar cell architectures," *Nano Energy*, vol. 98, Jul. 2022, doi: 10.1016/j.nanoen.2022.107221.

[25] J. Haschke *et al.*, "The impact of silicon solar cell architecture and cell interconnection on energy yield in hot & sunny climates," *Energy Environ Sci*, vol. 10, no. 5, pp. 1196–1206, 2017, doi: 10.1039/c7ee00286f.

[26] Amir Asgharzadeh, Chris Deline, Joshua Stein, and Fatima Toor, "A Comparison Study of the Performance of South/North-facing vs East/West-facing Bifacial Modules under Shading Conditions," p. 541, 2018.

[27] Z. Zhang *et al.*, “The mathematical and experimental analysis on the steady-state operating temperature of bifacial photovoltaic modules,” *Renew Energy*, vol. 155, pp. 658–668, Aug. 2020, doi: 10.1016/j.renene.2020.03.121.

[28] A. Radwan, M. Mahmoud, A. G. Olabi, A. Rezk, H. M. Maghrabie, and M. A. Abdelkareem, “Thermal comparison of mono-facial and bi-facial photovoltaic cells considering the effect of TPT layer absorptivity,” *International Journal of Thermofluids*, vol. 18, May 2023, doi: 10.1016/j.ijft.2023.100306.

[29] F. Johansson, B. E. Gustafsson, B. Stridh, and P. E. Campana, “3D-thermal modelling of a bifacial agrivoltaic system: a photovoltaic module perspective,” *Energy Nexus*, vol. 5, Mar. 2022, doi: 10.1016/j.nexus.2022.100052.

[30] G. M. Tina, F. B. Scavo, and A. Gagliano, “Multilayer Thermal Model for Evaluating the Performances of Monofacial and Bifacial Photovoltaic Modules,” *IEEE J Photovolt*, vol. 10, no. 4, pp. 1035–1043, Jul. 2020, doi: 10.1109/JPHOTOV.2020.2982117.

[31] S. P. Aly, J. J. John, G. Mathiak, O. Albadwawi, L. Pomares, and V. Alberts, “A thermal model for bifacial PV panels,” in *Conference Record of the IEEE Photovoltaic Specialists Conference*, Institute of Electrical and Electronics Engineers Inc., 2022, pp. 457–459. doi: 10.1109/PVSC48317.2022.9938549.

[32] U. A. Yusufoglu *et al.*, “Simulation of energy production by bifacial modules with revision of ground reflection,” in *Energy Procedia*, Elsevier Ltd, 2014, pp. 389–395. doi: 10.1016/j.egypro.2014.08.111.

[33] G. J. M. Janssen, B. B. Van Aken, A. J. Carr, and A. A. Mewe, “Outdoor Performance of Bifacial Modules by Measurements and Modelling,” in *Energy Procedia*, Elsevier Ltd, 2015, pp. 364–373. doi: 10.1016/j.egypro.2015.07.051.

[34] C. D. Rodríguez-Gallegos, M. Bieri, O. Gandhi, J. P. Singh, T. Reindl, and S. K. Panda, “Monofacial vs bifacial Si-based PV modules: Which one is more cost-effective?,” *Solar Energy*, vol. 176, pp. 412–438, Dec. 2018, doi: 10.1016/j.solener.2018.10.012.

[35] M. H. Shahverdian, H. Sayyaadi, and A. Sohani, “A detailed optical thermo-electrical model for better thermal analysis of bifacial PV systems,” *Energy Conversion and Management: X*, vol. 24, Oct. 2024, doi: 10.1016/j.ecmx.2024.100817.

[36] M. Manni, S. Jouttijärvi, S. Ranta, K. Miettunen, and G. Lobaccaro, “Validation of model chains for global tilted irradiance on East-West vertical bifacial photovoltaics at high latitudes,” *Renew Energy*, vol. 220, Jan. 2024, doi: 10.1016/j.renene.2023.119722.

[37] J. F. Orgill and K. G. T Hollands, “Correlation equation for hourly diffuse radiation on a horizontal surface,” *Solar Energy*, vol. 19, pp. 357–359, 1977.

[38] D. G. Erbs, S. A. Klein, and J. A. Duffle, “Estimation of the diffuse radiation fraction for hourly, daily and monthly-average global radiation,” *Solar Energy*, vol. 28, no. 4, pp. 293–302, 1982.

[39] R. Perez, P. Ineichen, E. Maxwell, R. Seals, and A. Zelenka, “Dynamic global-to-direct irradiance conversion models,” *ASHRAE Trans*, vol. 98, no. 1, pp. 354–369, 1992, [Online]. Available: https://www.researchgate.net/publication/279868352

[40] D. T. Reindl, W. A. Beckman, and J. A. Duffle, “Diffuse fraction correlations,” *Solar Energy*, vol. 45, no. 1, pp. 1–7, 1990.

[41] Sandia National Laboratories, “Hay and Davies Sky Diffuse Model.” Accessed: Oct. 31, 2024. [Online]. Available: https://pvpmc.sandia.gov/modeling-guide/1-weather-design-inputs/plane-of-array-poa-irradiance/calculating-poa-irradiance/poa-sky-diffuse/hay-and-davies-sky-diffuse-model/

[42] R. Perezt, R. Seals, R. Stewartt, and D. Menicucci, “A new simplified version of the perez diffuse irradiance model for tilted surfaces Author links open overlay panel,” *Solar Energy*, vol. 39, no. 3, pp. 221–231, 1987.

[43] D. T. Reindl, W. A. Beckman, and J. A. Duffie, “Evaluation of hourly tilted surface radiation models,” *Solar Energy*, vol. 45, no. 1, pp. 9–17, 1990.

[44] Sandia National Laboratories, “Isotropic Sky Diffuse Model.” Accessed: Oct. 31, 2024. [Online]. Available: https://pvpmc.sandia.gov/modeling-guide/1-weather-design-inputs/plane-of-array-poa-irradiance/calculating-poa-irradiance/poa-sky-diffuse/isotropic-sky-diffuse-model/

[45] B. Sun, L. Lu, Y. Yuan, and P. Ocłoń, “Development and validation of a concise and anisotropic irradiance model for bifacial photovoltaic modules,” *Renew Energy*, vol. 209, pp. 442–452, Jun. 2023, doi: 10.1016/j.renene.2023.04.012.

[46] C. A. Gueymard and J. A. Ruiz-Arias, “Extensive worldwide validation and climate sensitivity analysis of direct irradiance predictions from 1-min global irradiance,” Apr. 01, 2016, *Elsevier Ltd*. doi: 10.1016/j.solener.2015.10.010.

[47] D. Yang, “Estimating 1-min beam and diffuse irradiance from the global irradiance: A review and an extensive worldwide comparison of latest separation models at 126 stations,” May 01, 2022, *Elsevier Ltd*. doi: 10.1016/j.rser.2022.112195.

[48] M. Ş. Kalay, B. Kılıç, and Ş. Sağlam, “Systematic review of the data acquisition and monitoring systems of photovoltaic panels and arrays,” Sep. 15, 2022, *Elsevier Ltd.* doi: 10.1016/j.solener.2022.08.029.

[49] D. L. King, W. E. Boyson, and J. A. Kratochvil, “Photovoltaic array performance model,” 2004. doi: https://doi.org/10.2172/919131.

[50] D. Faiman, “Assessing the outdoor operating temperature of photovoltaic modules,” *Progress in Photovoltaics: Research and Applications*, vol. 16, no. 4, pp. 307–315, Jun. 2008, doi: 10.1002/pip.813.

[51] M. Mattei, G. Notton, C. Cristofari, M. Muselli, and P. Poggi, “Calculation of the polycrystalline PV module temperature using a simple method of energy balance,” *Renew Energy*, vol. 31, no. 4, pp. 553–567, Apr. 2006, doi: 10.1016/j.renene.2005.03.010.

[52] E. Skoplaki and J. A. Palyvos, “Operating temperature of photovoltaic modules: A survey of pertinent correlations,” *Renew Energy*, vol. 34, no. 1, pp. 23–29, Jan. 2009, doi: 10.1016/j.renene.2008.04.009.

[53] E. Skoplaki, A. G. Boudouvis, and J. A. Palyvos, “A simple correlation for the operating temperature of photovoltaic modules of arbitrary mounting,” *Solar Energy Materials and Solar Cells*, vol. 92, no. 11, pp. 1393–1402, Nov. 2008, doi: 10.1016/j.solmat.2008.05.016.

[54] T. Townsend, “A method for estimating the long-term performance of direct-coupled photovoltaic systems,” University of Wisconsin-Madison, 1989.

[55] Sandia National Laboratories, “POA Beam.” Accessed: Oct. 31, 2024. [Online]. Available: https://pvpmc.sandia.gov/modeling-guide/1-weather-design-inputs/plane-of-array-poa-irradiance/calculating-poa-irradiance/poa-beam/

[56] D. L. King, J. A. Kratochvil, and W. E. Boyson, “Measuring solar spectral and angle-of-incidence effects on photovoltaic modules and solar irradiance sensors,” in *26th IEEE Photovoltaic Specialists Conference*, IEEE, Sep. 1997.

[57] Sandia National Laboratories, “Perez Sky Diffuse Model.” Accessed: Oct. 31, 2024. [Online]. Available: https://pvpmc.sandia.gov/modeling-guide/1-weather-design-inputs/plane-of-array-poa-irradiance/calculating-poa-irradiance/poa-sky-diffuse/perez-sky-diffuse-model/

[58] R. Perez, P. Ineichen, R. Seals, J. Michalsky, and R. Stewart, “Modeling daylight availability and irradiance components from direct and global irradiance,” *Solar Energy*, vol. 44, no. 5, pp. 271–289, 1990.

[59] H. Böök, A. Poikonen, A. Aarva, T. Mielonen, M. R. A. Pitkänen, and A. V. Lindfors, “Photovoltaic system modeling: A validation study at high latitudes with implementation of a novel DNI quality control method,” *Solar Energy*, vol. 204, pp. 316–329, Jul. 2020, doi: 10.1016/j.solener.2020.04.068.

[60] J. Varjopuro, A. Kamppinen, A. Poskela, J. A. Karhu, A. V. Lindfors, and K. Miettunen, “Comparison of Perovskite and Silicon Solar Panel Temperatures in Varying Ambient Conditions by Computational Simulation,” *Submitted to Solar Energy Materials and Solar Cells*.

[61] J. Zhou, Q. Yi, Y. Wang, and Z. Ye, “Temperature distribution of photovoltaic module based on finite element simulation,” *Solar Energy*, vol. 111, pp. 97–103, Jan. 2015, doi: 10.1016/j.solener.2014.10.040.

[62] T. Sobota, “Fourier’s Law of Heat Conduction,” in *Encyclopedia of Thermal Stresses*, R. B. Hetnarski, Ed., Springer, 2014. doi: 10.1007/978-94-007-2739-7_384.

[63] A. Mills, *Heat and Mass Transfer*. 1995. doi: 10.4324/9780203752173.

[64] J. Watmuff, D. Proctor, and S. Australia, “Solar and wind induced external coefficients-Solar collectors,” 2017. [Online]. Available: https://www.researchgate.net/publication/234355019

[65] J. Zhou, Q. Yi, Y. Wang, and Z. Ye, “Temperature distribution of photovoltaic module based on finite element simulation,” *Solar Energy*, vol. 111, pp. 97–103, 2015, doi: 10.1016/j.solener.2014.10.040.

[66] G. Notton, C. Cristofari, M. Mattei, and P. Poggi, “Modelling of a double-glass photovoltaic module using finite differences,” *Appl Therm Eng*, vol. 25, no. 17–18, pp. 2854–2877, 2005, doi: 10.1016/j.applthermaleng.2005.02.008.

[67] Y. Lee and A. A. O. Tay, “Finite element thermal analysis of a solar photovoltaic module,” in *Energy Procedia*, 2012, pp. 413–420. doi: 10.1016/j.egypro.2012.02.050.

[68] M. A. Green, “Intrinsic concentration, effective densities of states, and effective mass in silicon,” *J Appl Phys*, vol. 67, no. 6, pp. 2944–2954, 1990.

[69] L. C. Hirst and N. J. Ekins-Daukes, “Fundamental losses in solar cells,” *Progress in Photovoltaics: Research and Applications*, vol. 19, no. 3, pp. 286–293, May 2011, doi: 10.1002/pip.1024.

[70] L. V. Mercaldo and P. D. Veneri, “Silicon solar cells: Materials, technologies, architectures,” in *Solar Cells and Light Management: Materials, Strategies and Sustainability*, Elsevier, 2019, pp. 35–57. doi: 10.1016/B978-0-08-102762-2.00002-1.

[71] J. Haschke *et al.*, “The impact of silicon solar cell architecture and cell interconnection on energy yield in hot & sunny climates,” *Energy Environ Sci*, vol. 10, no. 5, pp. 1196–1206, 2017, doi: 10.1039/c7ee00286f.

[72] F. F. Muhammadsharif and S. Hashim, “A Simple and Efficient Determination of the Ideality Factor of Solar Cells and Modules from the Knee Point of the Shunt Resistance Curve,” *Arab J Sci Eng*, vol. 48, no. 6, pp. 8217–8225, Jun. 2023, doi: 10.1007/s13369-023-07860-3.

[73] C. Berthod, R. Strandberg, G. H. Yordanov, H. G. Beyer, and J. O. Odden, “On the Variability of the Temperature Coefficients of mc-Si Solar Cells with Irradiance,” in *Energy Procedia*, Elsevier Ltd, Aug. 2016, pp. 2–9. doi: 10.1016/j.egypro.2016.07.002.

[74] I. Subedi, T. J. Silverman, M. G. Deceglie, and N. J. Podraza, “PERC silicon PV infrared to ultraviolet optical model,” *Solar Energy Materials and Solar Cells*, vol. 215, Sep. 2020, doi: 10.1016/j.solmat.2020.110655.

[75] Sandia National Laboratories, “PVLIB Toolbox.” Accessed: Oct. 31, 2024. [Online]. Available: https://pvpmc.sandia.gov/tools/pv_lib-toolbox/

[76] N. Martin and J. M. Ruiz, “Calculation of the PV modules angular losses under "eld conditions by means of an analytical model,” 2001.

[77] N. Martín and J. M. Ruiz, “Annual angular reflection losses in PV modules,” *Progress in Photovoltaics: Research and Applications*, vol. 13, no. 1, pp. 75–84, Jan. 2005, doi: 10.1002/pip.585.

[78] M. B. Øgaard, H. N. Riise, H. Haug, S. Sartori, and J. H. Selj, "Photovoltaic system monitoring for high latitude locations," *Solar Energy*, vol. 207, pp. 1045–1054, Sep. 2020, doi: 10.1016/j.solener.2020.07.043.

[79] M. Koehl, M. Heck, S. Wiesmeier, and J. Wirth, "Modeling of the nominal operating cell temperature based on outdoor weathering," *Solar Energy Materials and Solar Cells*, vol. 95, no. 7, pp. 1638–1646, Jul. 2011, doi: 10.1016/j.solmat.2011.01.020.

[80] M. Grisanti *et al.*, "Thermal Models of Monofacial and Bifacial PV Modules: Machine Learning and Physical Estimation Models Comparison," in *Conference Record of the IEEE Photovoltaic Specialists Conference*, Institute of Electrical and Electronics Engineers Inc., 2023. doi: 10.1109/PVSC48320.2023.10360013.

[81] J. D. Mondol, Y. G. Yohanis, and B. Norton, "Comparison of measured and predicted long term performance of grid a connected photovoltaic system," *Energy Convers Manag*, vol. 48, no. 4, pp. 1065–1080, Apr. 2007, doi: 10.1016/j.enconman.2006.10.021.

[82] B. Quesada, C. Sánchez, J. Cañada, R. Royo, and J. Payá, "Experimental results and simulation with TRNSYS of a 7.2kWp grid-connected photovoltaic system," *Appl Energy*, vol. 88, no. 5, pp. 1772–1783, 2011, doi: 10.1016/j.apenergy.2010.12.011.

[83] R. Bharti, J. Kuitche, and M. G. Tamizhmani, "Nominal Operating Cell Temperature (NOCT): Effects of module size, loading and solar spectrum," *Conference Record of the IEEE Photovoltaic Specialists Conference*, pp. 001657–001662, 2009, doi: 10.1109/PVSC.2009.5411408.

[84] M. Akhsassi *et al.*, "Experimental investigation and modeling of the thermal behavior of a solar PV module," *Solar Energy Materials and Solar Cells*, vol. 180, pp. 271–279, Jun. 2018, doi: 10.1016/j.solmat.2017.06.052.